

**Thin-film flow of a viscoplastic material
round a large horizontal stationary
or rotating cylinder**

A. B. Ross, S. K. Wilson* and B. R. Duffy†

Department of Mathematics,
University of Strathclyde,
Livingstone Tower,
26 Richmond Street,
Glasgow G1 1XH,
United Kingdom

August 11, 2000

*Email : s.k.wilson@strath.ac.uk, Telephone : + 44 (0) 141 548 3820, Fax : + 44 (0) 141 552

8657

†Email : b.r.duffy@strath.ac.uk, Telephone : + 44 (0) 141 548 3645, Fax : + 44 (0) 141 552

8657

Abstract

In this paper we consider the steady two-dimensional thin-film flow of a viscoplastic material, modelled as a biviscosity fluid with a yield stress, round the outside of a large horizontal stationary or rotating cylinder. In both cases we determine the leading-order solution both when the ratio of the viscosities in the ‘yielded’ and ‘unyielded’ regions is of order unity and when this ratio approaches zero in the appropriate distinguished limit. When the viscosity ratio is of order unity the flow consists, in general, of a region of yielded fluid adjacent to the cylinder and a region of unyielded fluid adjacent to the free surface, separated by the yield surface. In the distinguished limit the flow consists, in general, of a region of yielded fluid adjacent to the cylinder whose stress is significantly above the yield stress and a pseudo-plug region adjacent to the free surface, in which the leading-order azimuthal component of velocity is independent of the radial coordinate but varies azimuthally, separated by the pseudo-yield surface; the pseudo-plug region is itself, in general, divided by the yield surface into a region of yielded fluid whose stress is only just above the yield stress and an unyielded region adjacent to the free surface. The solution for a stationary cylinder represents a curtain of fluid with prescribed volume flux falling onto the top of and off at the bottom of the cylinder. If the flux is sufficiently small then the flow is unyielded everywhere, but when it exceeds a critical value there is a yielded region. In the distinguished limit the yielded region always extends all the way round the cylinder, but the unyielded region does so only when the flux is sufficiently small. For a rotating cylinder a solution representing a film with finite thickness everywhere is possible only when the flux is sufficiently small. Depending on the value of the flux and the speed of rotation the flow may be

unyielded everywhere, have a yielded region on the right of the cylinder only, or have yielded regions on both the right and left of the cylinder. At the critical maximum flux the maximum supportable weight of fluid on the cylinder is attained and the pseudo-yield, yield and free surfaces all have a corner. In the distinguished limit there are rigid plugs (absent in the stationary case) near the top and bottom of the cylinder.

1 Introduction

A great number of materials, ranging from many of the paints and inks used in industrial coating applications to numerous muds and lavas found in geophysical contexts, are ‘viscoplastic’, that is to say they behave essentially like rigid solids when subjected to a small stress but flow readily (‘yield’) when subjected to a large stress. Various constitutive equations have been proposed to model these viscoplastic materials; for an overview of such models and the types of flow problems that have been considered see the comprehensive review articles by Bird, Dai & Yarusso (1983) and Barnes (1999).

Much of the literature involving flow of viscoplastics has concentrated on the idealised case of a ‘Bingham’ material, that is, a material that behaves like a perfectly rigid solid ‘plug’ unless the stress exceeds the yield stress, but otherwise behaves like a viscous fluid. For example, Bird *et al.* (1983) considered rectilinear flow of a Bingham material with rigid plugs in various geometries, Lipscomb & Denn (1984) and Tichy (1991) considered thin-film flow in various confined geometries, while Liu & Mei (1989, 1994), Huang & García (1997) and Balmforth & Craster (1999) investigated thin-film flow down an inclined plane. A generalisation of the Bingham model is the Herschel-Bulkley model, and thin-film flow of a Herschel-Bulkley material down an inclined

plane has recently been investigated by Coussot (1994), Coussot & Proust (1996), Di Federico (1998), Huang & García (1998) and Balmforth & Craster (1999).

Recent advances in experimental techniques (see, for example, Barnes 1999) have revealed that the concept of a well-defined yield stress below which no flow occurs enshrined in the Bingham model is rather idealised, and that typically materials flow very slowly even at very low stresses, that is, there is in reality no well-defined yield stress. Nevertheless, the Bingham model has proved to be a very useful one in a wide range of practical applications. However, even in steady two-dimensional flow, the use of the Bingham model for thin-film flows is not without its complications. As many authors have pointed out, a naive treatment of non-rectilinear flows gives rise to the so-called ‘Bingham paradox’, namely that regions of material that appear to have a stress below the yield stress (and which are therefore supposed to behave like a rigid plug) are found to be deforming. Evidently, as Lipscomb & Denn (1984) pointed out, perfectly rigid plugs are possible only in strictly rectilinear flow. An additional complication of using the Bingham model is that by assuming that any unyielded regions are perfectly rigid we deprive ourselves of any means of determining the stresses within them.

In an important recent paper Balmforth & Craster (1999) demonstrated that the earlier work by Walton & Bittleston (1991) on rectilinear axial flow of a Bingham material through a narrow eccentric annulus contained the essence of the resolution of the Bingham paradox. Balmforth & Craster (1999) showed that, when interpreted correctly, the Bingham model does in fact lead to a consistent description of non-rectilinear thin-film flow. In particular, Balmforth & Craster’s (1999) careful asymptotic analysis of non-rectilinear thin-film flow of a Bingham material down an inclined plane in the limit $\epsilon \rightarrow 0$, where ϵ (defined in §3) is the aspect ratio of the film, reveals that the solu-

tion consists of two regions, namely a region of yielded fluid adjacent to the substrate (called the ‘fully plastic’ region by Balmforth & Craster 1999) in which the stress is significantly (specifically $O(1)$) above the yield stress, and a region of yielded fluid adjacent to the free surface (called the ‘pseudo-plug’ region by Walton & Bittleston 1991 and Balmforth & Craster 1999) in which the leading-order longitudinal component of velocity is independent of the transverse coordinate but varies with the longitudinal coordinate and in which the stress is only just (specifically $O(\epsilon)$) above the yield stress; these two regions are separated by an apparent yield surface (called the ‘pseudo-yield surface’ by Walton & Bittleston 1991 and the ‘fake yield surface’ by Balmforth & Craster 1999). Since in the non-rectilinear flow considered by Balmforth & Craster (1999) the stress in the fluid is everywhere above the yield stress the entire flow is yielded and hence the apparent paradox disappears. Moreover, this analysis also reveals that the pseudo-yield surface is precisely the same as the ‘yield surface’ calculated from the naive approach, and so the apparently paradoxical solutions obtained by earlier authors can in fact be justified by identifying the ‘unyielded regions’ as pseudo-plug regions and the ‘yield surfaces’ as pseudo-yield surfaces. Pseudo-plug regions of this kind were also obtained by O’Donovan & Tanner (1984) in their numerical investigation of axisymmetric squeeze flow, as well as by Walton & Bittleston (1991) and Beverly & Tanner (1992) in their analytical and numerical studies of rectilinear axial flow in a narrow eccentric annulus.

At the same time as Balmforth & Craster (1999) were undertaking their analysis Wilson (1999) independently performed a more general version of the same calculation using the more realistic biviscosity model (which permits flow below the ‘yield stress’ and in which the stresses within any unyielded regions are determined) instead

of the idealised Bingham model. Wilson's (1999) study of pressure-driven flow in a non-parallel-sided symmetric channel resolves the difficulties in the earlier (incomplete) analyses by Liu & Mei (1990), Wilson (1993) and Burgess & Wilson (1996) of, respectively, flow down an inclined plane, axisymmetric squeeze-film flow between parallel discs and axisymmetric spin coating. Specifically, Wilson (1999) adopted a biviscosity model with a yield stress from which the familiar Newtonian model is recovered in the case $\lambda = 1$ and the Bingham model is recovered in the limit $\lambda \rightarrow 0$, where λ (defined in §2) is a ratio of viscosities in the 'yielded' and 'unyielded' regions, which are separated by the 'yield surface' on which the stress is equal to the yield stress. In particular, Wilson (1999) investigated the distinguished limit $\lambda \rightarrow 0$ (the Bingham limit) and $\epsilon \rightarrow 0$ (the thin-film limit) in which $k = \epsilon/\lambda = O(1)$. In this limit the solution again has, in general, a yielded region adjacent to the substrate in which the stress is significantly (specifically $O(1)$) above the yield stress separated by a pseudo-yield surface from a pseudo-plug region adjacent to the free surface in which the leading-order longitudinal component of velocity is independent of the transverse coordinate but varies with the longitudinal coordinate. However, unlike in the case of a Bingham material, the pseudo-plug is now, in general, divided into a yielded region adjacent to the pseudo-yield surface in which the stress is just (specifically $O(\epsilon)$) above the yield stress, and an unyielded region adjacent to the free surface in which the stress is significantly (specifically $O(1)$) below the yield stress, these two regions being separated by the yield surface. The location of the yield surface (but not that of the pseudo-yield surface) depends on k . In the limit $k \rightarrow 0$ (corresponding to taking the thin-film limit $\epsilon \rightarrow 0$ and then the Bingham limit $\lambda \rightarrow 0$) the yield surface coincides with the pseudo-yield surface and so the yielded part of the pseudo-plug is absent,

while in the limit $k \rightarrow \infty$ (corresponding to taking the Bingham limit $\lambda \rightarrow 0$ and then the thin-film limit $\epsilon \rightarrow 0$) the unyielded part of the pseudo-plug is absent and the results of Balmforth & Craster (1999) for a Bingham material are recovered. It is, however, important to realise that Balmforth & Craster's (1999) work shows that it is not necessary to 'relax' the Bingham model in this or any other way in order to resolve the Bingham paradox.

We remark that Balmforth & Craster's (1999) and Wilson's (1999) analyses also provide the correct solution to the problem of thin-film flow of a Bingham material in a symmetric contraction treated in the recent paper by Gans (1999) (who used an inconsistent assumption about the velocity of the rigid plug he believed to be present in the contraction and hence obtained an erroneous solution there).

In this paper we consider the steady two-dimensional thin-film flow of a viscoplastic material, modelled as a biviscosity fluid with a yield stress (described in §2), round a large horizontal stationary or rotating cylinder. The corresponding Newtonian problems were investigated by Nusselt (1916*a,b*), Moffatt (1977) and Duffy & Wilson (1999). The biviscosity model used by Wilson (1999) is preferred to the idealised Bingham model used by Walton & Bittleston (1991) and Balmforth & Craster (1999) firstly because it is a more realistic model for real viscoplastic materials and secondly because it allows the stresses within any unyielded regions to be determined without making any additional ad hoc assumptions. In §3 we obtain the leading-order solutions in the case $\lambda = O(1)$ as $\epsilon \rightarrow 0$ and in the distinguished limit $\lambda \rightarrow 0$ and $\epsilon \rightarrow 0$ in which $k = \epsilon/\lambda = O(1)$. We then employ these solutions to describe flow round a stationary cylinder in §4 and §5, and round a rotating cylinder in §6 and §7. We summarise our results in §8.

2 A biviscosity fluid

The governing equations representing conservation of mass and balance of momentum for steady slow flow of an incompressible fluid with constant density ρ take the form

$$\nabla \cdot \mathbf{u} = 0, \quad \nabla \cdot \boldsymbol{\sigma} + \rho \mathbf{g} = \mathbf{0}, \quad (1)$$

where \mathbf{u} , $\boldsymbol{\sigma}$ and \mathbf{g} denote the fluid velocity, stress tensor and acceleration due to gravity, respectively. In the present work we shall consider a biviscosity fluid with a yield stress whose constitutive law is given by

$$\boldsymbol{\sigma} = -p\mathbf{I} + \boldsymbol{\sigma}', \quad \text{where} \quad \boldsymbol{\sigma}' = \begin{cases} 2\mu_1 \mathbf{e}, & \tau \leq \tau_y, \\ 2 \left(\mu_2 + \frac{\tau_0}{q} \right) \mathbf{e}, & \tau > \tau_y, \end{cases} \quad (2)$$

in which p is the pressure, \mathbf{I} is the identity tensor, \mathbf{e} is the rate-of-deformation tensor, q is the local shear rate and τ is a scalar measure of the local stress, given by

$$\mathbf{e} = \frac{1}{2} [(\nabla \mathbf{u}) + (\nabla \mathbf{u})^T], \quad q = [2 \operatorname{tr}(\mathbf{e}^2)]^{\frac{1}{2}}, \quad \tau = \left[\frac{1}{2} \operatorname{tr}(\boldsymbol{\sigma}'^2) \right]^{\frac{1}{2}}. \quad (3)$$

The other five quantities in (2), namely μ_1 , μ_2 , τ_0 , τ_y and q_y , are constant material parameters related by

$$\tau_y = \mu_1 q_y = \mu_2 q_y + \tau_0 \quad (4)$$

(so that only three of the five are independent). The parameters μ_1 and μ_2 are viscosities, and τ_0 and τ_y are measures of stress; τ_y is the yield stress, corresponding to the shear rate q_y . The relation between τ and q is given by

$$\tau = \begin{cases} \mu_1 q, & q \leq q_y, \\ \mu_2 q + \tau_0, & q > q_y, \end{cases} \quad (5)$$

and this is illustrated in figure 1; τ is a continuous piecewise-linear function of q with a discontinuity in slope at $q = q_y$. We note that $\tau_0 = \tau_y (1 - \lambda)$, where the viscosity

ratio λ is defined by $\lambda = \mu_2/\mu_1$. For $\tau \leq \tau_y$ the fluid is ‘unyielded’ and behaves like a Newtonian fluid with a ‘high’ (constant) viscosity μ_1 , while for $\tau > \tau_y$ the fluid is ‘yielded’ and behaves like a viscous fluid with a ‘low’ (shear-rate dependent) viscosity $\mu_2 + \tau_0/q$. In the present viscoplastic context $\mu_2 \leq \mu_1$ and so $0 < \lambda \leq 1$. Any surface on which $\tau = \tau_y$ which separates yielded and unyielded regions is called a ‘yield surface’. The familiar case of a Newtonian fluid with constant viscosity is recovered in the case $\lambda = 1$ and the Bingham model is recovered in the limit $\lambda \rightarrow 0$.

3 Problem formulation

Consider the steady two-dimensional flow of the viscoplastic material described in §2 round the outside of a large horizontal cylinder of radius R . We shall consider both the case when the cylinder is stationary and the case when it is rotating in a counter-clockwise sense about its horizontal axis with constant angular speed Ω (so that the circumferential speed is $U = R\Omega$). Hereafter all quantities will be made dimensionless using the radial length scale $h_y = \tau_y/\rho g$, the azimuthal length scale R , the azimuthal velocity scale $\rho g h_y^2/\mu_2$ and the stress scale τ_y . Provided that the fluid film is sufficiently slender, that is, provided that the aspect ratio of the film $\epsilon = h_y/R$ is sufficiently small, the leading-order approximation to the local behaviour is simply that of rectilinear flow (see, for example, Nusselt 1916*a,b* and Moffatt 1977) with volume flux Q on a locally planar substrate inclined at an angle $\alpha = \pi/2 - \theta$ to the horizontal and moving parallel to itself with constant speed U , where θ is the conventional polar angle measured anti-clockwise from the horizontal, as shown in figure 2. Referred to the local Cartesian co-ordinate system $Oxyz$ shown in figure 2, the substrate has velocity $U \geq 0$ in the

direction Ox and the local components of the fluid velocity in the directions Ox and Oz are denoted by u and w respectively.

3.1 The solution in the case $\lambda = O(1)$

When the viscosity ratio λ is of order unity as the aspect ratio ϵ approaches zero equations (2) and (3) give $\tau = |\sigma_{xz}|$ and $q = |du/dz|$ at leading order. In general, the solution in this case comprises a region $0 \leq z < H$ of yielded fluid (region 2) and a region $H \leq z \leq h$ of unyielded fluid (region 1), where the leading-order locations of the yield surface and the free surface are denoted by $z = H(\theta)$ and $z = h(\theta)$, respectively. The geometry of the local problem in this case is shown in figure 2(a). We define the term ‘yielded zone’ to correspond to those values of θ at which region 2 is present; at other values of θ (the ‘unyielded zone’) region 2 is absent and the fluid is unyielded across the entire thickness of the film.

At leading order in the yielded zone the governing equations (1) with the constitutive equation (2) reduce to simply

$$u_{1,x} + w_{1,z} = 0, \quad (6)$$

$$\lambda^{-1}u_{1,zz} = \cos \theta, \quad (7)$$

$$p_{1,z} = -\sin \theta \quad (8)$$

in region 1 and to

$$u_{2,x} + w_{2,z} = 0, \quad (9)$$

$$u_{2,zz} = \cos \theta, \quad (10)$$

$$p_{2,z} = -\sin \theta \quad (11)$$

in region 2. Equations (6)–(11) are subject to the boundary conditions

$$p_1 = 0 \quad \text{on} \quad z = h \quad (12)$$

$$u_{1,z} = 0 \quad \text{on} \quad z = h, \quad (13)$$

$$u_2 = U \quad \text{on} \quad z = 0, \quad (14)$$

$$u_1 = u_2 \quad \text{on} \quad z = H, \quad (15)$$

$$p_1 = p_2 \quad \text{on} \quad z = H, \quad (16)$$

$$\lambda^{-1}u_{1,z} = u_{2,z} - (1 - \lambda)S \quad \text{on} \quad z = H, \quad (17)$$

where $S = -\text{sgn}(u_{2,z})$; these represent continuity of normal stress and tangential stress on the free surface, no slip on the cylinder, and continuity of velocity, normal stress and tangential stress at the yield surface respectively. The yield condition, $\tau = 1$ on $z = H$, gives

$$|u_{1,z}| = |u_{2,z}| = \lambda \quad \text{on} \quad z = H. \quad (18)$$

Thus we obtain the hydrostatic pressure distribution

$$p = (h - z) \sin \theta \quad (19)$$

throughout the fluid, and the velocity distributions

$$u_1 = U - \frac{\lambda \cos \theta}{2}(2h - z)z - \frac{(1 - \lambda)}{2} [(2h - H) \cos \theta - 2S] H, \quad H \leq z \leq h, \quad (20)$$

$$u_2 = U - \frac{\cos \theta}{2}(2h - z)z + S(1 - \lambda)z, \quad 0 \leq z < H, \quad (21)$$

in regions 1 and 2 respectively. The volume flux of fluid, given by

$$Q = \int_0^H u_2 \, dz + \int_H^h u_1 \, dz, \quad (22)$$

is therefore

$$Q = Uh - \frac{\cos \theta}{3} [\lambda (h - H)^3 + h^3 - (h - H)^3] - \frac{S(1 - \lambda)}{2} (H - 2h) H. \quad (23)$$

The yield condition (18) gives

$$1 = (h - H)|\cos \theta|. \quad (24)$$

The streamfunctions $\psi_i = \psi_i(z)$ for $i = 1, 2$, defined by $u_i = \partial\psi_i/\partial z$ and satisfying $\psi_2(0) = 0$, $\psi_1(H) = \psi_2(H)$ and $\psi_1(h) = Q$, are given by

$$\begin{aligned} \psi_1(z) = & Uz - \frac{\lambda \cos \theta}{6}(3h - z)z^2 - \frac{(1 - \lambda)}{2} [(2h - H) \cos \theta - 2S] Hz \\ & + \frac{(1 - \lambda)}{6} [(3h - 2H) \cos \theta - 3S] H^2, \quad H \leq z \leq h, \end{aligned} \quad (25)$$

$$\psi_2(z) = Uz - \frac{\cos \theta}{6}(3h - z)z^2 + \frac{S(1 - \lambda)}{2} z^2, \quad 0 \leq z < H. \quad (26)$$

From (2) the stress throughout the fluid is given by

$$\tau = |\sigma_{xz}| = (h - z)|\cos \theta|, \quad (27)$$

from which it can be shown that $S = -\text{sgn}(u_{1,z}) = \text{sgn}(\cos \theta)$, so that the velocity gradient across the entire thickness of the film takes the opposite sign from $\cos \theta$.

At leading order in the unyielded zone we recover the appropriately non-dimensionalised version of the familiar solution for a Newtonian fluid with viscosity μ_1 , namely

$$u = U - \frac{\lambda \cos \theta}{2}(2h - z)z, \quad Q = Uh - \frac{\lambda \cos \theta}{3}h^3, \quad \psi = Uz - \frac{\lambda \cos \theta}{6}(3h - z)z^2, \quad (28)$$

as given, for example, by Moffatt (1977).

3.2 The solution in the distinguished limit $k = \epsilon/\lambda = O(1)$

In the distinguished asymptotic limit in which both the viscosity ratio λ and the aspect ratio ϵ approach zero with $k = \epsilon/\lambda = O(1)$ the situation is somewhat more complicated. As Wilson (1999) describes, in general the solution in this limit has three regions rather

than the two regions present in the case $\lambda = O(1)$. In $0 \leq z < H^*$ (region 2) the fluid is yielded with $u_z = O(1)$, in $H^* \leq z < H$ (region 3) the fluid is yielded with $u_z = O(\epsilon)$ and in $H \leq z \leq h$ (region 1) the fluid is unyielded with $u_z = O(\epsilon)$, where $z = H(\theta)$ and $z = h(\theta)$ are the yield surface and free surface encountered previously, and $z = H^*(\theta)$ is the ‘pseudo-yield surface’ at which u_z changes from $O(\epsilon)$ to $O(1)$. The geometry of the local problem in this case is shown in figure 2(b). As we shall see, the stress in region 3 is only $O(\epsilon)$ above the yield stress. We will refer to regions 1 and 3, in which the leading-order solution for u is independent of z but varies with θ , as a ‘pseudo plug’ in order to distinguish them from a rigid plug in which the velocity is constant. The definitions of the yielded and unyielded zones are as before; however, in this case the yielded zone will comprise, in general, both ‘partially yielded zones’ (in which regions 1, 2 and 3 are present) and ‘fully yielded zones’ (in which only regions 2 and 3 are present). The details of the solution are given in the Appendix, and show that in the yielded zone H^* , H and h satisfy

$$Q = Uh - \frac{\cos \theta}{6}(3h - H^*)H^{*2}, \quad (29)$$

$$(h - H^*)|\cos \theta| = 1, \quad (30)$$

$$(h - H)^2 \cos^2 \theta + k^2 \left[\frac{d}{d\theta} \{H^{*2} \cos \theta\} \right]^2 = 1. \quad (31)$$

Equations (29), (30) and (31) are the volume flux, pseudo-yield and yield conditions, respectively, and are equivalent to the corresponding equations derived by Wilson (1999) (namely, his equation (9), his condition $Gy_c = 1$ and his equation (7), respectively) for pressure-driven thin-film flow of a biviscosity fluid in a non-parallel-sided symmetric channel.

In the special case $k = 0$ (corresponding to taking the thin-film limit $\epsilon \rightarrow 0$ and

then the Bingham limit $\lambda \rightarrow 0$) we have $H^* \equiv H$ so that region 3 is absent and the problem reduces to that when $\lambda = O(1)$ in the special case $\lambda = 0$, while in the special case $k = \infty$ (corresponding to taking the Bingham limit $\lambda \rightarrow 0$ and then the thin-film limit $\epsilon \rightarrow 0$) only regions 2 and 3 are present.

Both H^* and h are independent of k . Moreover, equations (23) and (24) in the special case $\lambda = 0$ are equivalent to (29) and (30) when H is replaced by H^* , and so the solutions for the free surface h and the pseudo-yield surface H^* in the distinguished limit are identical to those for the free surface h and the yield surface H that are obtained by setting $\lambda = 0$ in the solution for $\lambda = O(1)$. In particular, setting $\lambda = 0$ in (28) confirms that in this case the solution in the unyielded zone is simply a rigid plug; we shall subsequently find that these occur only for flow on a rotating cylinder ($U \neq 0$).

4 Stationary cylinder ($U = 0$) when $\lambda = O(1)$

In this section we consider the solution when $\lambda = O(1)$ as $\epsilon \rightarrow 0$ in the special case $U = 0$ corresponding to thin-film flow with prescribed volume flux Q round a stationary cylinder. For ease of comparison with the earlier work on this problem (and to distinguish between the present results and those for a rotating cylinder which follow) we present all the results for a stationary cylinder in terms of the local angle to the horizontal α (defined in §3) instead of the polar angle θ . To obtain the appropriate equations from the general ones given in §3 we set $U = 0$ and $\theta = \pi/2 - \alpha$ and replace u and Q with $-u$ and $-Q$ respectively. In this case, just as Nusselt (1916*a,b*) found in the Newtonian case, the only physically acceptable solution corresponds to a curtain

of fluid falling onto the top ($\alpha = 0$) of and falling off at the bottom ($\alpha = \pi$) of the cylinder. When a flux Q_s of fluid is supplied from above the cylinder a portion Q will flow round the right-hand side ($0 < \alpha < \pi$) and the remainder $Q_s - Q$ will flow round the left-hand side ($-\pi < \alpha < 0$) of the cylinder. As Duffy & Wilson (1999) point out in their recent study of thin-film and curtain flow of a Newtonian fluid on a horizontal cylinder, the fluxes Q and $Q_s - Q$ need not be equal, and so the overall flow need not have left-to-right symmetry. However, without loss of generality we restrict our attention to flow round the right side of the cylinder in what follows; the corresponding flow on the left side can then be calculated in the same way with Q replaced by $Q_s - Q$.

Eliminating H between (23) and (24) gives a cubic polynomial equation for h in the yielded zone, namely

$$h^3 - \frac{3(1-\lambda)}{2\sin\alpha}h^2 + \frac{1-\lambda}{2\sin^3\alpha} - \frac{3Q}{\sin\alpha} = 0. \quad (32)$$

If we define

$$K = 1 - \frac{2}{(1-\lambda)^2} + \frac{12Q\sin^2\alpha}{(1-\lambda)^3} \quad (33)$$

then from (32) the only physically acceptable solution for the free surface h is

$$h = \begin{cases} \frac{1-\lambda}{2\sin\alpha} \left[1 + 2\cos\left(\frac{1}{3}\cos^{-1}K\right) \right], & -1 \leq K \leq 1, \\ \frac{1-\lambda}{2\sin\alpha} \left[1 + 2\cosh\left(\frac{1}{3}\cosh^{-1}K\right) \right], & K > 1. \end{cases} \quad (34)$$

The yield surface H is then given by (24), so that

$$H = h - \frac{1}{\sin\alpha}. \quad (35)$$

Note that H and h depend on α only through $\sin\alpha$ and so the solution has a top-to-bottom symmetry. From (32) and (35) we have

$$h' = -\frac{\cos\alpha [h^3 \sin^3\alpha - (1-\lambda)]}{3h \sin^3\alpha [h \sin\alpha - (1-\lambda)]} \quad (36)$$

and

$$H' = -\frac{\cos \alpha [h^3 \sin^3 \alpha - 3h^2 \sin^2 \alpha + 3(1 - \lambda)h \sin \alpha - (1 - \lambda)]}{3h \sin^3 \alpha [h \sin \alpha - (1 - \lambda)]}, \quad (37)$$

where the dash denotes $d/d\alpha$.

The edges of the yielded zone are where the yield surface H meets the cylinder, that is, where $H = 0$ and (from (35)) $h = 1/\sin \alpha$. Thus from (32) the yielded zone is $\alpha_e < \alpha < \pi - \alpha_e$, where α_e ($0 \leq \alpha_e \leq \pi/2$) is given by

$$\alpha_e = \sin^{-1} \left[\left(\frac{\lambda}{3Q} \right)^{\frac{1}{2}} \right], \quad (38)$$

and so

$$h(\alpha_e) = \left(\frac{3Q}{\lambda} \right)^{\frac{1}{2}}. \quad (39)$$

Thus from (38) a yielded zone is present only if

$$Q > \frac{\lambda}{3}, \quad (40)$$

that is, only if Q is sufficiently large.

In the unyielded zone we have from (28)

$$u = \frac{\lambda \sin \alpha}{2} (2h - z)z, \quad h = \left(\frac{3Q}{\lambda \sin \alpha} \right)^{\frac{1}{3}}, \quad \psi = \frac{\lambda \sin \alpha}{6} (3h - z)z^2, \quad (41)$$

as given, for example, by Nusselt (1916*a,b*).

From (36) and (41) it can be shown that h takes its minimum value at $\alpha = \pi/2$ and increases monotonically away from $\alpha = \pi/2$, becoming infinite at $\alpha = 0$ and $\alpha = \pi$. From (37) we find that H may have either a local maximum or a local minimum at $\alpha = \pi/2$. The flow is always unyielded when α is near 0 and π and thus from (41) we have

$$h = \left(\frac{3Q}{\lambda \alpha} \right)^{\frac{1}{3}} + O(\alpha^{\frac{5}{3}}) \quad (42)$$

as $\alpha \rightarrow 0$, with the corresponding behaviour near $\alpha = \pi$.

In the limit $Q \rightarrow 0$ the fluid is unyielded everywhere and the flow is described by (41). In the limit $Q \rightarrow \infty$ we have

$$\alpha_e = \left(\frac{\lambda}{3Q} \right)^{\frac{1}{2}} + O(Q^{-\frac{3}{2}}) \quad (43)$$

and

$$H = \left(\frac{3Q}{\sin \alpha} \right)^{\frac{1}{3}} - \frac{1 + \lambda}{2 \sin \alpha} + O(Q^{-\frac{1}{3}}), \quad (44)$$

$$h = \left(\frac{3Q}{\sin \alpha} \right)^{\frac{1}{3}} + \frac{1 - \lambda}{2 \sin \alpha} + O(Q^{-\frac{1}{3}}). \quad (45)$$

The latter two expansions are non-uniform when $\alpha = O(Q^{-1/2})$, that is, when α is of the same order as α_e . These non-uniformities are resolved by appropriate inner solutions in which H increases from zero at $\alpha = \alpha_e$ to the $O(Q^{1/3})$ value given in (44) and h decreases from the $O(Q^{1/2})$ value given in (39) at $\alpha = \alpha_e$ to the $O(Q^{1/3})$ value given in (45).

There are two distinct flow topologies in this case. If $Q \leq \lambda/3$ then the flow is unyielded everywhere (type I), while if $Q > \lambda/3$ then there is a yielded zone (type II); typical examples of these two different flows (with streamlines included) are shown in figure 3. In particular, figure 3(b) shows that some streamlines lie entirely in the unyielded region whereas others enter and exit the yielded region, confirming that the yield surface is not a material surface.

Figures 4 and 5 show H and h plotted as functions of α/π for a range of values of λ and Q , respectively. Figures 4 and 5 illustrate that both H and h at each station around the cylinder and the extent of the yielded zone increase both when λ is decreased for fixed Q and when Q is increased for fixed λ . Note that only in the special case $\lambda = 0$

(included in figure 4) does the yielded zone extend all the way around the cylinder. In the special case $\lambda = 1$ (also included in figure 4) the ‘yield surface’ H merely represents a surface in the fluid on which the stress takes the yield value of unity and the fluid undergoes no material change there since the viscosity is the same in the yielded and unyielded regions in this special case.

Evidently h is continuous at $\alpha = \alpha_e$. Furthermore, (36) and (41) show that h' is also continuous at $\alpha = \alpha_e$ and is given by

$$h'(\alpha_e) = -\frac{Q \cos \alpha_e}{\lambda}, \quad (46)$$

while from (37)

$$H'(\alpha_e) = \frac{2Q \cos \alpha_e}{\lambda}. \quad (47)$$

Note from (46) and (47) that $h'(\alpha_e) < 0$ and $H'(\alpha_e) > 0$ with $H'(\alpha_e)$ increasing and $h'(\alpha_e)$ decreasing as Q is increased or λ is decreased, in agreement with the results shown in figures 4 and 5. In contrast, h'' is, in general, discontinuous at $\alpha = \alpha_e$. Specifically, $\Delta h''(\alpha_e) = h''(\alpha_e^+) - h''(\alpha_e^-)$ is given by

$$\Delta h''(\alpha_e) = -\frac{4}{9\lambda^2} \left(\frac{3Q}{\lambda} \right)^{\frac{1}{2}} (1 - \lambda)(3Q - \lambda) \quad (48)$$

and is plotted as a function of λ for a range of values of Q in figure 6; in particular, figure 6 illustrates that $\Delta h''(\alpha_e)$ is an increasing function of λ and a decreasing function of Q . This discontinuity in h'' accounts for the lack of smoothness of the free surface at $\alpha = \alpha_e$ just evident in figure 3(b) and in figure 4 in the case $\lambda = 1/10$.

Near $\alpha = \pi/2$ we find that H and h are given by

$$H = H_0 + H_2 \left(\alpha - \frac{\pi}{2} \right)^2 + O \left(\alpha - \frac{\pi}{2} \right)^4, \quad (49)$$

$$h = h_0 + h_2 \left(\alpha - \frac{\pi}{2} \right)^2 + O \left(\alpha - \frac{\pi}{2} \right)^4, \quad (50)$$

where from (35) we have $H_0 = h_0 - 1$ and $H_2 = h_2 - 1/2$, with h_0 given by (34) evaluated at $\alpha = \pi/2$, and

$$h_2 = -\frac{(1-\lambda)(h_0^2-1)+2Q}{4h_0(1-\lambda-h_0)}. \quad (51)$$

In particular, if $H_2 = 0$ then $Q = Q_M$, where $Q_M = Q_M(\lambda)$ is given parametrically by

$$\lambda = \frac{(h_0-1)^3}{3h_0-1}, \quad Q_M = \frac{h_0^2(h_0^2-1)(h_0-1)}{2(3h_0-1)}, \quad (52)$$

with $1 < h_0 \leq 3$ in order that $0 < \lambda \leq 1$. Thus if $\lambda/3 < Q < Q_M$ then H has a local maximum, while if $Q > Q_M$ then H has a local minimum at $\alpha = \pi/2$. Figure 7 shows how the curves $Q = \lambda/3$ and $Q = Q_M$ divide the (λ, Q) parameter plane into regions in which the flow is of type I, the flow is of type II with a maximum in H (labelled II_{\max}) and the flow is of type II with a minimum in H (labelled II_{\min}). This behaviour is illustrated by the results shown in figures 4 and 5.

Also of interest is the (finite) weight of fluid on the cylinder. To leading order the weight on the right-hand side of the cylinder is given by

$$W(\lambda, Q) = \int_0^\pi h(\alpha) \, d\alpha. \quad (53)$$

Figure 8 shows a plot of W as a function of Q for a range of values of λ . Note that W can be made arbitrarily large by making λ sufficiently small or Q sufficiently large.

The special case $\lambda = 0$

The solution in the special case $\lambda = 0$ is of particular interest. With (35) equations (20), (21) and (23) reduce to

$$u_1 = \frac{H^2 \sin \alpha}{2}, \quad H \leq z \leq h, \quad (54)$$

$$u_2 = \frac{\sin \alpha}{2}(2H - z)z, \quad 0 \leq z < H, \quad (55)$$

$$Q = \frac{H^3 \sin \alpha}{3} + \frac{H^2}{2}, \quad (56)$$

where H and h are given by setting $\lambda = 0$ in (35) and (34). In this case the velocity in region 1 is independent of z (but not α) and $\alpha_e = 0$, that is, the unyielded zone is absent. We note that

$$H = (2Q)^{\frac{1}{2}} - \frac{2Q}{3}\alpha + O(\alpha^2), \quad (57)$$

$$h = \frac{1}{\alpha} + (2Q)^{\frac{1}{2}} + \frac{(1 - 4Q)}{6}\alpha + O(\alpha^2) \quad (58)$$

as $\alpha \rightarrow 0$,

$$H = (2Q)^{\frac{1}{2}} - \frac{2 \sin \alpha}{3}Q + \frac{5\sqrt{2} \sin^2 \alpha}{9}Q^{\frac{3}{2}} - \frac{32 \sin^3 \alpha}{27}Q^2 + O(Q^{\frac{5}{2}}), \quad (59)$$

$$h = \frac{1}{\sin \alpha} + (2Q)^{\frac{1}{2}} - \frac{2 \sin \alpha}{3}Q + \frac{5\sqrt{2} \sin^2 \alpha}{9}Q^{\frac{3}{2}} - \frac{32 \sin^3 \alpha}{27}Q^2 + O(Q^{\frac{5}{2}}) \quad (60)$$

as $Q \rightarrow 0$ (we shall need to know these latter expansions to the given accuracy in §5.3), and

$$H = \left(\frac{3Q}{\sin \alpha} \right)^{\frac{1}{3}} - \frac{1}{2 \sin \alpha} + O(Q^{-\frac{1}{3}}), \quad (61)$$

$$h = \left(\frac{3Q}{\sin \alpha} \right)^{\frac{1}{3}} + \frac{1}{2 \sin \alpha} + O(Q^{-\frac{1}{3}}) \quad (62)$$

as $Q \rightarrow \infty$. Evidently (61) and (62) are non-uniform when $\alpha = O(Q^{-1/2})$. These non-uniformities are resolved by the inner solutions

$$H = H_0 Q^{\frac{1}{2}} + \frac{H_0^2 \hat{\alpha}^3}{18(1 + H_0 \hat{\alpha})} Q^{-\frac{1}{2}} + O(Q^{-\frac{3}{2}}), \quad (63)$$

$$h = \left[H_0 + \frac{1}{\hat{\alpha}} \right] Q^{\frac{1}{2}} + \left[\frac{H_0^2 \hat{\alpha}^3}{18(1 + H_0 \hat{\alpha})} + \frac{\hat{\alpha}}{6} \right] Q^{-\frac{1}{2}} + O(Q^{-\frac{3}{2}}), \quad (64)$$

where we have written $\alpha = \hat{\alpha}Q^{-1/2}$ and H_0 is the appropriate solution of the cubic equation

$$\frac{H_0^3 \hat{\alpha}}{3} + \frac{H_0^2}{2} = 1. \quad (65)$$

5 Stationary cylinder ($U = 0$) when $k = O(1)$

In this section we consider the solution in the distinguished limit $\lambda \rightarrow 0$ and $\epsilon \rightarrow 0$ in which $k = \epsilon/\lambda = O(1)$ in the special case $U = 0$, corresponding to thin-film flow with prescribed volume flux Q round a stationary cylinder. The calculations in the Appendix show that in the yielded zone H^* , H and h satisfy

$$Q = \frac{\sin \alpha}{6}(3h - H^*)H^{*2}, \quad (66)$$

$$(h - H^*) \sin \alpha = 1, \quad (67)$$

$$(h - H)^2 \sin^2 \alpha + k^2 \left[\frac{d}{d\alpha} \{H^{*2} \sin \alpha\} \right]^2 = 1. \quad (68)$$

Both H^* and h are independent of k . Using (67) to eliminate h from (66) yields

$$Q = \frac{H^{*3} \sin \alpha}{3} + \frac{H^{*2}}{2}. \quad (69)$$

Since equations (67) and (69) are identical to (35) and (56) with H replaced by H^* the solutions for h and H^* in this case are identical to those for h and H in the case $\lambda = 0$, respectively. The edges of the yielded zone are where the pseudo-yield surface H^* meets the cylinder, and are at $\alpha = \alpha_e^*$ and $\alpha = \pi - \alpha_e^*$, where α_e^* is identical to α_e in the case $\lambda = 0$. Hence all the results for H , h and $\alpha_e (= 0)$ in the case $\lambda = 0$ given in §4 apply directly to H^* , h and $\alpha_e^* (= 0)$ in the present problem. Of course, this does not mean that other quantities (such as, for example, the stress) are the same. Solving (68) yields

$$H = h - \frac{1}{\sin \alpha} \left[1 - \left(k \frac{d}{d\alpha} \{H^{*2} \sin \alpha\} \right)^2 \right]^{\frac{1}{2}}, \quad (70)$$

where, from (69),

$$\frac{d}{d\alpha} \{H^{*2} \sin \alpha\} = \frac{(3 + H^* \sin \alpha)H^{*2} \cos \alpha}{3(1 + H^* \sin \alpha)}. \quad (71)$$

Combining (70) and (71) shows that H^* , H and h depend on α only through $\sin \alpha$ and so, as in the case $\lambda = O(1)$ considered in §4, they always have top-to-bottom symmetry. Note that $H^* = H$ when $\alpha = \pi/2$, and so region 3 is always absent at this special value of α .

Although H^* and h always extend from $\alpha = 0$ to $\alpha = \pi$, the same is not necessarily true for H ; specifically, we find that if $Q > 1/2k$ then the yield surface H meets the free surface h , at $\alpha = \alpha_e$ and $\alpha = \pi - \alpha_e$, where α_e ($0 \leq \alpha_e \leq \pi/2$) is the (unique) solution of

$$k \frac{d}{d\alpha} \{H^{*2} \sin \alpha\} = 1. \quad (72)$$

If $Q \leq 1/2k$ then

$$H = \begin{cases} \frac{1}{\alpha} \left[1 - (1 - 4k^2Q^2)^{\frac{1}{2}} \right] + (2Q)^{\frac{1}{2}} \left[1 - \frac{16k^2Q^2}{3(1 - 4k^2Q^2)^{\frac{1}{2}}} \right] + O(\alpha), & Q < \frac{1}{2k}, \\ \frac{1}{\alpha} - \frac{1}{k^{\frac{1}{4}}} \left(\frac{8}{3\alpha} \right)^{\frac{1}{2}} + \frac{1}{k^{\frac{1}{2}}} + O(\alpha^{\frac{1}{2}}), & Q = \frac{1}{2k}, \end{cases} \quad (73)$$

as $\alpha \rightarrow 0$, while if $Q > 1/2k$ then

$$H = h(\alpha_e) - \frac{(\alpha - \alpha_e)^{\frac{1}{2}}}{\sin \alpha_e} \left[-2k \frac{d^2}{d\alpha^2} \{H^{*2} \sin \alpha\} \right]_{\alpha=\alpha_e}^{\frac{1}{2}} + O(\alpha - \alpha_e) \quad (74)$$

as $\alpha \rightarrow \alpha_e^+$. All three surfaces always have a global minimum at $\alpha = \pi/2$.

There are two distinct flow topologies in this case. If $Q \leq 1/2k$ then there is only a partially yielded zone (type II₁), while if $Q > 1/2k$ then there are a partially yielded zone and two fully yielded zones (type II₂); typical examples of these two different flows are shown in figure 9. In particular, figure 9(a) shows that fluid particles start (at $\alpha = 0$) and finish (at $\alpha = \pi$) in the pseudo-plug (regions 1 and 3), but may pass through the yielded region (region 2), whilst figure 9(b) shows that all particles start and finish in region 3, but must, in general, pass through either region 1 or region 2.

Figures 10, 11 and 12 show H^* , H and h plotted as functions of α/π for various values of Q and k .

5.1 The limit $k \rightarrow 0$

In the limit $k \rightarrow 0$ we have

$$H = H_0 + k^2 H_2 + O(k^4), \quad (75)$$

where $H_0 = H^*$ and

$$H_2 = \frac{1}{2 \sin \alpha} \left(\frac{d}{d\alpha} \{H^{*2} \sin \alpha\} \right)^2. \quad (76)$$

In particular,

$$H_2 = \frac{2Q^2}{\alpha} - \frac{16(2Q^5)^{\frac{1}{2}}}{3} + O(\alpha) \quad (77)$$

as $\alpha \rightarrow 0$, and comparing (57) and (77) shows that (75) is non-uniform when $\alpha = O(k^2)$.

This non-uniformity is resolved by the inner solution

$$H = (2Q)^{\frac{1}{2}} + \frac{2Q^2}{\hat{\alpha}} + \frac{2Q}{3\hat{\alpha}}(3Q^3 - 8\sqrt{2}Q^{\frac{3}{2}}\hat{\alpha} - \hat{\alpha}^2)k^2 + O(k^4), \quad (78)$$

where we have written $\alpha = k^2 \hat{\alpha}$.

5.2 The limit $k \rightarrow \infty$

In the limit $k \rightarrow \infty$ we have

$$\alpha_e = \frac{\pi}{2} - \frac{3(1 + H_0^*)}{H_0^{*2}(3 + H_0^*)} \frac{1}{k} + O\left(\frac{1}{k^2}\right), \quad (79)$$

where $H_0^* = H^*(\pi/2)$, and the behaviour of H^* , H and h in the partially yielded zone is given by

$$H^* = H_0^* + O\left(\frac{1}{k^2}\right), \quad (80)$$

$$H = 1 + H_0^* - \left[1 - \left(\frac{\frac{\pi}{2} - \alpha}{\frac{\pi}{2} - \alpha_e} \right)^2 \right]^{\frac{1}{2}} + O\left(\frac{1}{k^2}\right), \quad (81)$$

$$h = 1 + H_0^* + O\left(\frac{1}{k^2}\right). \quad (82)$$

Figure 13 shows a sketch of the leading-order solution in the partially yielded zone in which h and H^* are constant (independent of α) whereas H has a semi-elliptical shape with width $O(k^{-1})$ and unit height.

5.3 The limit $Q \rightarrow 0$

In the limit $Q \rightarrow 0$ we find that H^* and h are given by (59) and (60) respectively and that

$$H = (2Q)^{\frac{1}{2}} - \frac{2 \sin \alpha}{3} Q + \frac{5\sqrt{2} \sin^2 \alpha}{9} Q^{\frac{3}{2}} + \left(\frac{2k^2 \cos^2 \alpha}{\sin \alpha} - \frac{32 \sin^3 \alpha}{27} \right) Q^2 + O(Q^{\frac{5}{2}}). \quad (83)$$

Comparison of (83) with (59) shows that H^* and H differ at $O(Q^2)$ in this limit. The solution for H (but not that for H^* or h) is not uniformly valid when $\alpha = O(Q^{1/2})$. This non-uniformity is resolved by an appropriate inner solution near $\alpha = 0$, but, since it appears first only at $O(Q^{3/2})$, we do not pursue the details here.

5.4 The limit $Q \rightarrow \infty$

In the limit $Q \rightarrow \infty$ we find that H^* and h are given by (61) and (62) respectively. Furthermore,

$$\alpha_e = \frac{\pi}{2} - \frac{3^{\frac{1}{3}}}{k} Q^{-\frac{2}{3}} + O(Q^{-\frac{1}{2}}), \quad (84)$$

and the behaviour of H^* , H and h in the partially yielded zone is given by

$$H^* = (3Q)^{\frac{1}{3}} - \frac{1}{2} + O(Q^{-\frac{1}{3}}), \quad (85)$$

$$H = (3Q)^{\frac{1}{3}} + \frac{1}{2} - \left[1 - \left(\frac{\frac{\pi}{2} - \alpha}{\frac{\pi}{2} - \alpha_e} \right)^2 \right]^{\frac{1}{2}} + O(Q^{-\frac{1}{3}}), \quad (86)$$

$$h = (3Q)^{\frac{1}{3}} + \frac{1}{2} + O(Q^{-\frac{1}{3}}). \quad (87)$$

Figure 14 shows a sketch of the first-order-accurate solution in the partially yielded zone in which H^* and h are constant (independent of α) whereas H has a semi-elliptical shape with width $O(Q^{-2/3})$ and unit height.

6 Rotating cylinder ($U \neq 0$) when $\lambda = O(1)$

In this section we consider the solution when $\lambda = O(1)$ as $\epsilon \rightarrow 0$ in the general case $U \neq 0$ corresponding to thin-film flow with volume flux Q round a rotating cylinder. In this case, just as Duffy & Wilson (1999) found in the Newtonian case, there are two physically acceptable solutions, one corresponding to a film of finite non-zero thickness everywhere (the solution studied in the Newtonian case by Moffatt 1977) and another corresponding to a curtain of fluid falling onto the top of and off at the bottom of the cylinder (studied in the Newtonian case by Duffy & Wilson 1999). In this work we shall be concerned exclusively with the former solution. Note that this solution is absent in the special case $U = 0$ treated earlier, and so the following results do not, in general, reduce to those given in §4 and §5 in the limit $U \rightarrow 0$.

Eliminating H from (23) by using (24) gives a cubic polynomial equation for h in the yielded zone, namely

$$h^3 - \frac{3(1-\lambda)}{2|\cos\theta|}h^2 - \frac{3U}{\cos\theta}h + \frac{(1-\lambda)}{2|\cos\theta|^3} + \frac{3Q}{\cos\theta} = 0. \quad (88)$$

If we define

$$K = \frac{1}{|M|^{\frac{3}{2}}} [(1 - \lambda)^3 - 2(1 - \lambda)(1 - 3U \cos \theta) - 12SQ \cos^2 \theta], \quad (89)$$

where

$$M = (1 - \lambda)^2 + 4U \cos \theta, \quad (90)$$

then from (88) the appropriate solution for the free surface h is

$$h = \frac{1 - \lambda}{2 \cos \theta} + \frac{M^{\frac{1}{2}}}{\cos \theta} \cos \left(\frac{2\pi}{3} - \frac{1}{3} \cos^{-1} K \right), \quad -1 \leq K \leq 1, \quad (91)$$

on the right ($S = 1$), and

$$h = \begin{cases} \frac{1 - \lambda}{2|\cos \theta|} + \frac{|M|^{\frac{1}{2}}}{|\cos \theta|} \sinh \left(\frac{1}{3} \sinh^{-1} K \right), & M \leq 0, \\ \frac{1 - \lambda}{2|\cos \theta|} + \frac{M^{\frac{1}{2}}}{|\cos \theta|} \cos \left(\frac{1}{3} \cos^{-1} K \right), & M > 0 \quad \text{and} \quad -1 \leq K \leq 1, \\ \frac{1 - \lambda}{2|\cos \theta|} + \frac{M^{\frac{1}{2}}}{|\cos \theta|} \cosh \left(\frac{1}{3} \cosh^{-1} K \right), & M > 0 \quad \text{and} \quad K > 1, \end{cases} \quad (92)$$

on left ($S = -1$). The yield surface H is given by (24). Note that H and h have top-to-bottom symmetry as in the case $U = 0$, but now they do not have left-to-right symmetry, and so hereafter the subscripts R and L will be used to denote quantities on the right ($S = 1$) and left ($S = -1$), respectively, when necessary. The solution (91) is physically sensible only if $K \geq -1$ throughout the yielded zone, and in particular if $K \geq -1$ at $\theta = 0$, that is, if $Q \leq Q_C$, where

$$Q_C = \frac{1}{12} \left[(1 - \lambda)^3 - 2(1 - \lambda)(1 - 3U) + [(1 - \lambda)^2 + 4U]^{\frac{3}{2}} \right]. \quad (93)$$

From (88) and (24) we have

$$h' = -\frac{\sin \theta [h^3 \cos^3 \theta - S(1 - \lambda)]}{3 \cos^3 \theta [U + S(1 - \lambda)h - h^2 \cos \theta]} \quad (94)$$

and

$$H' = -\frac{\sin \theta [h^3 \cos^3 \theta - 3Sh^2 \cos^2 \theta + 3(1 - \lambda)h \cos \theta + 3SU \cos \theta - S(1 - \lambda)]}{3 \cos^3 \theta [U + S(1 - \lambda)h - h^2 \cos \theta]} \quad (95)$$

(where the dash denotes $d/d\theta$) except at $\theta = 0$ in the case $Q = Q_C$; this special case is considered later. From (94) it can be shown that $h' \leq 0$ on the top half of the cylinder and $h' \geq 0$ on the bottom half of the cylinder. Hence τ takes its maximum value of $h(0)$ at $z = 0$, $\theta = 0$ and so there can be a region of yielded fluid only if $h(0) > 1$. From (91) it is clear that $h(0)$ is maximised when $Q = Q_C$ (corresponding to $K = -1$), and a necessary condition for yielded zones to exist is therefore

$$U > \lambda. \quad (96)$$

For $U \leq \lambda$ the flow is unyielded everywhere.

As before, the edges of the yielded zone are where the yield surface H meets the cylinder, that is, where $H = 0$ and (from (24)) $h = 1/|\cos \theta|$. Thus from (88) the yielded zones on the right and left are given by $|\theta| < \theta_{eR}$ and $|\pi - \theta| < \pi - \theta_{eL}$, respectively, where θ_{eR} ($0 \leq \theta_{eR} \leq \pi/2$) and θ_{eL} ($\pi/2 \leq \theta_{eL} \leq \pi$) are given by

$$\theta_e = \cos^{-1} \left[\frac{SU}{2Q} \left(1 + \left\{ 1 - \frac{4S\lambda Q}{3U^2} \right\}^{\frac{1}{2}} \right) \right], \quad (97)$$

and so

$$h(\theta_e) = \frac{3SU}{2\lambda} \left(1 - \left\{ 1 - \frac{4S\lambda Q}{3U^2} \right\}^{\frac{1}{2}} \right), \quad (98)$$

with the appropriate choice for S . Thus from (97) a yielded zone is present on the right only if

$$Q \leq \frac{3U^2}{4\lambda}, \quad Q > \frac{U}{2}, \quad Q > Q_R, \quad (99)$$

where

$$Q_R = U - \frac{\lambda}{3}. \quad (100)$$

Similarly, from (97) a yielded zone is present on the left only if $Q > Q_L$, where

$$Q_L = U + \frac{\lambda}{3} \geq Q_R. \quad (101)$$

From (97) we find that $\theta_{eR} \geq \pi - \theta_{eL}$ (with equality when $\lambda = 0$) and so the extent of the yielded zone is always greater on the right than on the left when $\lambda \neq 0$.

From (28) h in the unyielded zone satisfies

$$h^3 - \frac{3U}{\lambda \cos \theta} h + \frac{3Q}{\lambda \cos \theta} = 0. \quad (102)$$

If we define

$$K_N = -\frac{3SQ}{2} \left(\frac{\lambda |\cos \theta|}{U^3} \right)^{\frac{1}{2}} \quad (103)$$

then from (102) the appropriate solution for h is

$$h = 2 \left(\frac{U}{\lambda \cos \theta} \right)^{\frac{1}{2}} \cos \left(\frac{2\pi}{3} - \frac{1}{3} \cos^{-1} K_N \right), \quad -1 \leq K_N \leq 0, \quad (104)$$

on the right ($S = 1$), and

$$h = 2 \left(\frac{U}{\lambda |\cos \theta|} \right)^{\frac{1}{2}} \sinh \left(\frac{1}{3} \sinh^{-1} K_N \right), \quad K_N > 0, \quad (105)$$

on the left ($S = -1$). If the fluid is unyielded everywhere then (104) is physically sensible only if $Q \leq Q_N$, where

$$Q_N = \frac{2U^{\frac{3}{2}}}{3\lambda^{\frac{1}{2}}}, \quad (106)$$

in agreement with the result obtained by Moffatt (1977) in the Newtonian case, and from (102) we have

$$h' = -\frac{\lambda h^3 \sin \theta}{3(U - \lambda h^2 \cos \theta)}, \quad (107)$$

except at $\theta = 0$ in the case $Q = Q_N$.

From (94) and (107) it can be shown that h takes its maximum value at $\theta = 0$ and decreases monotonically away from $\theta = 0$ to its minimum value at $\theta = \pi$. From

(95) we find that H always has a local maximum at $\theta = 0$ but may have either a local maximum or a local minimum at $\theta = \pi$. The flow is always unyielded near $\theta = \pm\pi/2$, and thus from (102) we have

$$h = \frac{Q}{U} - \frac{\lambda Q^3}{3U^4} \left(\theta - \frac{\pi}{2} \right) + O \left(\theta - \frac{\pi}{2} \right)^2 \quad (108)$$

as $\theta \rightarrow \pi/2$, with the corresponding behaviour near $\theta = -\pi/2$.

As we have seen, yielded zones can exist only for $U > \lambda$ and in this case the strongest restrictions on Q are $Q > Q_R$, $Q \leq Q_C$ and $Q > Q_L$. For $U > \lambda$ we have $Q_R < Q_C < Q_N$, with $Q_R = Q_C = Q_N = 2\lambda/3$ when $U = \lambda$. There are therefore three distinct flow topologies. If $U \leq \lambda$ and $Q \leq Q_N$ or $U > \lambda$ and $Q \leq Q_R$ then the flow is unyielded everywhere (type I), if $U > \lambda$ and $Q_R < Q \leq \min(Q_C, Q_L)$ then there is a yielded zone on the right but not on the left (type II), while if $U > \lambda$ and $Q_L < Q \leq Q_C$ then there are yielded zones on both the right and left (type III); typical examples of these three different flows (with streamlines included) are shown in figure 15. Note that these definitions differ from those in §4. Figure 16 shows a plot of a typical (U, Q) parameter plane for a fixed value of λ (in this case $\lambda = 1/2$); in particular it shows how the curves $Q = Q_N$, $Q = Q_R$, $Q = Q_L$ and $Q = Q_C$ divide the parameter plane into a region where no solution exists and regions in which the three different types of flow occur.

Figures 17, 18 and 19 show H and h plotted as functions of θ/π for a range of values of λ , U and Q , respectively. Figure 17 illustrates that both H and h at each station round the cylinder and the extent of the yielded zone on the right increase and on the left decrease when λ is increased for fixed U and Q . Figure 18 illustrates that both H and h at each station round the cylinder and the extent of the yielded zone on

both the right and left decrease when U is increased for fixed λ and Q , while figure 19 illustrates the same behaviour when Q is decreased for fixed λ and U .

Evidently h is continuous at $\theta = \theta_e$. Furthermore, (94) and (107) show that h' is also continuous at $\theta = \theta_e$ and is given by

$$h'(\theta_e) = -\frac{S\lambda \sin \theta_e}{3 \cos^2 \theta_e (U \cos \theta_e - \lambda)}, \quad (109)$$

while from (95)

$$H'(\theta_e) = -\frac{S \sin \theta_e (3U \cos \theta_e - 2\lambda)}{3 \cos^2 \theta_e (U \cos \theta_e - \lambda)}. \quad (110)$$

As in the case $U = 0$ discussed in §4, h'' is, in general, discontinuous at $\theta = \theta_e$.

Also of interest is the local behaviour of H and h near $\theta = 0$, and in particular, the formation of corners in both surfaces at $\theta = 0$ when $Q = Q_C$, as shown in figures 17–19. When $Q_R < Q < Q_C$ we find that near $\theta = 0$ H and h are given by

$$H = H_0 + H_2\theta^2 + O(\theta^4), \quad (111)$$

$$h = h_0 + h_2\theta^2 + O(\theta^4), \quad (112)$$

where from (24) we have $H_0 = h_0 - 1$ and $H_2 = h_2 - 1/2$, with h_0 given by (91) evaluated at $\theta = 0$, and

$$h_2 = -\frac{(1 - \lambda)(h_0^2 - 1) + 2Uh_0 - 2Q}{4(U + (1 - \lambda)h_0 - h_0^2)}. \quad (113)$$

Since $h_2 < 0$ and $H_2 < 0$ both h and H always have a local maximum at $\theta = 0$. In the special case $Q = Q_C$ we find that near $\theta = 0$ H and h are given by

$$H = H_0 \mp A\theta + H_2\theta^2 + O(\theta^3), \quad (114)$$

$$h = h_0 \mp A\theta + h_2\theta^2 + O(\theta^3), \quad (115)$$

where

$$A = \left[\frac{h_0^3 + \lambda - 1}{3(2h_0 + \lambda - 1)} \right]^{\frac{1}{2}}, \quad h_2 = \frac{3h_0^2 - 2A^2}{6(2h_0 + \lambda - 1)}, \quad (116)$$

and where from (24) and (91) we have $H_0 = h_0 - 1$, $H_2 = h_2 - 1/2$ and

$$h_0 = \frac{1}{2} \left[1 - \lambda + ((1 - \lambda)^2 + 4U)^{\frac{1}{2}} \right], \quad (117)$$

showing that the profiles for both H and h have a corner at $\theta = 0$ with internal angle $\pi - 2A$ in this case. As $U \rightarrow \lambda^+$ we have $\theta_{\text{eR}} \rightarrow 0^+$, so that the extent of the yielded zone on the right decreases to zero. Both A and $h'(\theta_{\text{eR}})$ take the value $[U/3(1+U)]^{1/2}$ at $U = \lambda$. When $U \leq \lambda$ and $Q = Q_{\text{N}}$ (in which case the flow is unyielded everywhere) h has a corner at $\theta = 0$ with $A = (U/6\lambda)^{1/2}$, in agreement with the result for a Newtonian fluid (see, for example, Duffy & Wilson 1999). Hence for $\lambda \neq 1$ there is a finite jump in the value of A from $6^{-1/2}$ to $[U/3(1+U)]^{1/2}$ at $U = \lambda$. Figure 20 shows A and $h'(\theta_{\text{eR}})$ plotted as functions of U for a range of values of λ and, in particular, shows this jump. The special case $\lambda = 0$ is discussed later.

When $Q_{\text{L}} < Q \leq Q_{\text{C}}$ we find that near $\theta = \pi$ H and h are given by

$$H = H_0 + H_2(\theta - \pi)^2 + O(\theta - \pi)^4, \quad (118)$$

$$h = h_0 + h_2(\theta - \pi)^2 + O(\theta - \pi)^4, \quad (119)$$

where from (24) we have $H_0 = h_0 - 1$ and $H_2 = h_2 - 1/2$, with h_0 given by (92) evaluated at $\theta = \pi$, and

$$h_2 = \frac{(1 - \lambda)(h_0^2 - 1) - 2Uh_0 + 2Q}{4(U - (1 - \lambda)h_0 + h_0^2)}. \quad (120)$$

Since $h_2 > 0$ then h always has a local minimum at $\theta = \pi$. Defining Q_{M} such that $H_2 = 0$ when $Q = Q_{\text{M}}$ we find that if $Q_{\text{L}} < Q < \min(Q_{\text{M}}, Q_{\text{C}})$ then H has a local

maximum, whereas if $Q_M < Q \leq Q_C$ then H has a local minimum at $\theta = \pi$. Figure 21 shows a plot of the (U, Q) parameter plane for a fixed value of λ (in this case $\lambda = 1/2$) on a larger scale than figure 16, showing how the curve $Q = Q_M$ divides the region in which flows of type III occur into regions where H has a local maximum (labelled III_{\max}) or a local minimum (labelled III_{\min}).

One property of considerable practical interest is the maximum weight of fluid that can be supported on the rotating cylinder (first considered by Moffatt 1977 in the Newtonian case). To leading order the weight of fluid on the cylinder is given by

$$W(\lambda, U, Q) = \int_0^{2\pi} h(\theta) \, d\theta, \quad (121)$$

and figure 22 shows a plot of W as a function of Q for several values of U in the case $\lambda = 1/2$. As figure 22 shows, W increases monotonically (almost, but not exactly, linearly) with Q until it reaches the maximum supportable weight W_{\max} . This maximum weight is given by $W_{\max} = W(\lambda, U, Q_N)$ when $U \leq \lambda$ and $W_{\max} = W(\lambda, U, Q_C)$ when $U > \lambda$. Figure 23 shows a plot of W_{\max} as a function of U for a range of values of λ ; in particular, for $U > \lambda$ we have $W_{\max} > 4.44272$ whilst for $U < \lambda$ we have $W_{\max} < 4.44272$, and in the special case $U = \lambda$ we have $W_{\max} = 4.44272$, the (corrected) value obtained by Moffatt (1977) in the Newtonian case (see, for example, Duffy & Wilson 1999). The special case $\lambda = 0$ is discussed next.

The special case $\lambda = 0$

The special case $\lambda = 0$ is again of particular interest. In the yielded zone, using (24) in (20), (21) and (23) we have

$$u_1 = U - \frac{H^2 \cos \theta}{2}, \quad H \leq z \leq h, \quad (122)$$

$$u_2 = U - \frac{\cos \theta}{2}(2H - z)z, \quad 0 \leq z < H, \quad (123)$$

$$\frac{H^3 \cos \theta}{3} + \frac{H^2 S}{2} - UH - \frac{SU}{\cos \theta} + Q = 0, \quad (124)$$

with H and h given by setting $\lambda = 0$ in (24), (91) and (92). From (97) we have simply

$$\theta_e = \cos^{-1} \left[\frac{SU}{Q} \right], \quad (125)$$

and thus $\theta_{eR} = \pi - \theta_{eL}$ and so the extents of the yielded zones on the right and the left are the same. From (93), (100) and (101) we obtain

$$Q_C = \frac{1}{12} \left[6U - 1 + (1 + 4U)^{\frac{3}{2}} \right], \quad Q_R = Q_L = U. \quad (126)$$

In the unyielded zone we have simply

$$u = U, \quad h = \frac{Q}{U}, \quad (127)$$

that is, a rigid plug of uniform thickness Q/U moving with constant speed U . Since $Q_R = Q_L$ flows of type II do not occur in this case. Figure 24 shows how the curves $Q = Q_R = Q_L$ and $Q = Q_C$ divide the (U, Q) parameter plane in this case into a region where no solution exists and regions in which flows of type I and III occur. From (109), (110) and (124) we have $h'(\theta_e) = 0$,

$$H'(\theta_e) = -\frac{S \sin \theta_e}{\cos^2 \theta_e} = -\frac{SQ}{U^2} (Q^2 - U^2)^{\frac{1}{2}}, \quad (128)$$

and

$$H''(\theta_e) = \frac{Q}{U^5} (U^4 - SQU^2 - 2Q^2U^2 + SQ^3). \quad (129)$$

Figure 20 includes a plot of A as a function of U when $\lambda = 0$. Figure 23 includes a plot of W_{\max} as a function of U when $\lambda = 0$; in particular, as $U \rightarrow 0$ the solution approaches a rigid plug of thickness unity all the way round the cylinder and so $W_{\max} \rightarrow 2\pi$.

7 Rotating cylinder ($U \neq 0$) when $k = O(1)$

In this section we consider the solution in the distinguished limit $\lambda \rightarrow 0$ and $\epsilon \rightarrow 0$ in which $k = \epsilon/\lambda = O(1)$, in the general case $U \neq 0$ corresponding to thin-film flow with volume flux Q round a rotating cylinder. The calculations in the Appendix show that in the yielded zone H^* , H and h satisfy

$$Q = Uh - \frac{\cos \theta}{6}(3h - H^*)H^{*2}, \quad (130)$$

$$(h - H^*)|\cos \theta| = 1, \quad (131)$$

$$(h - H)^2 \cos^2 \theta + k^2 \left[\frac{d}{d\theta} \{H^{*2} \cos \theta\} \right]^2 = 1. \quad (132)$$

Both H^* and h are independent of k . Using (131) to eliminate h from (130) yields

$$\frac{H^{*3} \cos \theta}{3} + \frac{H^{*2}S}{2} - UH^* - \frac{SU}{\cos \theta} + Q = 0. \quad (133)$$

Since equations (131) and (133) are identical to (24) and (124) with H replaced by H^* the solutions for h and H^* in this case are again identical to those for h and H in the case $\lambda = 0$, respectively. The edges of the yielded zone are where the pseudo-yield surface H^* meets the cylinder, and are given by $|\theta| = \theta_{eR}^*$ and $|\pi - \theta| = \pi - \theta_{eL}^*$, where θ_{eR}^* and θ_{eL}^* are identical to θ_{eR} and θ_{eL} in the case $\lambda = 0$. Hence all the results for H , h and θ_e in the case $\lambda = 0$ given in §6 apply directly to H^* , h and θ_e^* in the present problem. Solving (132) yields

$$H = h - \frac{1}{|\cos \theta|} \left[1 - \left(k \frac{d}{d\theta} \{H^{*2} \cos \theta\} \right)^2 \right]^{\frac{1}{2}}, \quad (134)$$

where, from (133),

$$\frac{d}{d\theta} \{H^{*2} \cos \theta\} = \frac{H^* \sin \theta (H^{*3} \cos^2 \theta + 3SH^{*2} \cos \theta - 3UH^* \cos \theta - 6SU)}{3 \cos \theta (U - SH^* - H^{*2} \cos \theta)}, \quad (135)$$

except at $\theta = 0$ in the case $Q = Q_C$. Combining (134) and (135) shows that, as in the case $\lambda = O(1)$ considered in §6, H^* , H and h always have top-to-bottom but not left-to-right symmetry. Note that $H^* = H$ at $\theta = 0$ for $Q \neq Q_C$, at $\theta = \pi$ and at the edges of the yielded zones, and so region 3 is always absent at these special values of θ .

When $Q_R < Q < Q_C$ there are two critical values of k , denoted by k_{critR} and k_{critL} ($> k_{\text{critR}}$), such that if $k \geq k_{\text{critR}}$ then H meets h at $\theta = \pm\theta_{e1R}$ and $\theta = \pm\theta_{e2R}$ ($0 \leq \theta_{e1R} \leq \theta_{e2R} \leq \pi/2$) on the right, and if $k \geq k_{\text{critL}}$ then H meets h at $\theta = \pm\theta_{e1L}$ and $\theta = \pm\theta_{e2L}$ ($\pi/2 \leq \theta_{e2L} \leq \theta_{e1L} \leq \pi$) on the left, where θ_{e1} and θ_{e2} are the appropriate solutions of

$$k \frac{d}{d\theta} \{H^{*2} \cos \theta\} = 1. \quad (136)$$

As $\theta \rightarrow \theta_e^*$ from below and above on the right and left respectively we have

$$H = H_1(\theta - \theta_e^*) + H_2(\theta - \theta_e^*)^2 + O(\theta - \theta_e^*)^3, \quad (137)$$

where $H_1 = H_1^* = H^{*'}(\theta_e^*)$ is given by (128) and

$$H_2 = H_2^* + \frac{2Q^3 k^2}{U^7} (Q^2 - U^2)^2, \quad (138)$$

where $H_2^* = H^{*''}(\theta_e^*)/2$ is given by (129). If $k > k_{\text{crit}}$ then

$$H = h(\theta_{e1}) - \frac{S(-S(\theta - \theta_{e1}))^{\frac{1}{2}}}{\cos \theta_{e1}} \left[2Sk \frac{d^2}{d\theta^2} \{H^{*2} \cos \theta\} \right]_{\theta=\theta_{e1}}^{\frac{1}{2}} + O(\theta - \theta_{e1}) \quad (139)$$

as $\theta \rightarrow \theta_{e1}$ from below and above on the right and left respectively, and

$$H = h(\theta_{e2}) - \frac{S(S(\theta - \theta_{e2}))^{\frac{1}{2}}}{\cos \theta_{e2}} \left[-2Sk \frac{d^2}{d\theta^2} \{H^{*2} \cos \theta\} \right]_{\theta=\theta_{e2}}^{\frac{1}{2}} + O(\theta - \theta_{e2}) \quad (140)$$

as $\theta \rightarrow \theta_{e2}$ from above and below on the right and left respectively.

There are four distinct flow topologies in this case. If $Q \leq Q_R$ then the flow is of type I (a rigid plug of thickness Q/U), if $Q_R < Q < Q_C$ and $k < k_{\text{critR}}$ then the flow is of type III with only partially yielded zones on both the right and left (type III₁), if $Q_R < Q < Q_C$ and $k_{\text{critR}} < k < k_{\text{critL}}$ then the flow is of type III with both partially and fully yielded zones on the right but only a partially yielded zone on the left (type III₂), while if $Q_R < Q < Q_C$ and $k > k_{\text{critL}}$ then the flow is of type III with both partially and fully yielded zones on both the right and left (type III₃); typical examples of these different flows of type III are shown in figure 25. Figure 26 shows H^* , H and h plotted as functions of θ/π for various values of k for a value of Q satisfying $Q_R < Q < Q_C$.

For $Q_R < Q < Q_C$ we find that near $\theta = 0$ H is given by

$$H = H_0 + H_2\theta^2 + O(\theta^4), \quad (141)$$

where $H_0 = H_0^* = H^*(0)$ and

$$H_2 = H_2^* + \frac{H_0^{*2} (H_0^{*3} + 3H_0^{*2} - 3UH_0^* - 6U)^2 k^2}{18 (U - H_0^* - H_0^{*2})^2}, \quad (142)$$

where $H_2^* = H^{*''}(0)/2$. Thus H can have either a local maximum or a local minimum at $\theta = 0$. In the special case $Q = Q_C$ we have

$$\frac{d}{d\theta} \{H^{*2} \cos \theta\} = 2H_0^*A + O(\theta) \quad (143)$$

near $\theta = 0$, from which we find that if $k \geq k_{\text{critR}} (= 1/2H_0^*A$ when $Q = Q_C$) then H meets h at $\theta = \pm\theta_{\text{e1R}}$ ($0 \leq \theta_{\text{e1R}} \leq \pi/2$) on the right, where θ_{e1R} is the (unique) solution of (136); the behaviour on the left is as before. Note that, unlike when $k > k_{\text{critR}}$ for $Q_R < Q < Q_C$, H meets h only twice (as opposed to four times) when $k > k_{\text{critR}}$ for

$Q = Q_C$. For $k < k_{\text{critR}}$ near $\theta = 0$ H is given by

$$H = H_0^* + 1 - [1 - (2H_0^*Ak)^2]^{\frac{1}{2}} \mp B\theta + O(\theta^2), \quad (144)$$

where

$$B = A - \frac{2H_0^*Ak^2 (H_0^{*2} - 2A^2 - 4H_0^*H_2^*)}{[1 - (2H_0^*Ak)^2]^{\frac{1}{2}}}, \quad (145)$$

showing that the profile for H has a corner at $\theta = 0$ with internal angle $\pi - 2B$ in this case. Furthermore, unlike when $k < k_{\text{critR}}$ for $Q_R < Q < Q_C$ (in which case $H = H^*$ at $\theta = 0$), $H \neq H^*$ at $\theta = 0$ when $k < k_{\text{critR}}$ for $Q = Q_C$. Figure 27 shows H^* , H and h plotted as functions of θ/π for various values of k in the case $Q = Q_C$. Figure 28 shows a plot of B as a function of k for a range of values of U , and, in particular, shows that $B \rightarrow \infty$ as $k \rightarrow k_{\text{critR}}^-$, that is, the corner becomes a cusp as it approaches the free surface.

When $Q_R < Q \leq Q_C$ we find that near $\theta = \pi$ H is given by

$$H = H_0 + H_2(\theta - \pi)^2 + O(\theta - \pi)^4, \quad (146)$$

where $H_0 = H_0^* = H^*(\pi)$ and

$$H_2 = H_2^* + \frac{H_0^{*2} (H_0^{*3} + 3H_0^{*2} + 3UH_0^* + 6U)^2 k^2}{18 (U + H_0^* + H_0^{*2})^2}, \quad (147)$$

where $H_2^* = H^{*''}(\pi)/2$. Thus, if $Q_R < Q < \min(Q_M, Q_C)$ then H has either a local maximum or a local minimum at $\theta = \pi$, whereas if $Q_M < Q \leq Q_C$ then H always has a local minimum at $\theta = \pi$.

7.1 The limit $k \rightarrow 0$

In the limit $k \rightarrow 0$ we have

$$H = H_0 + k^2 H_2 + O(k^4), \quad (148)$$

where $H_0 = H^*$ and

$$H_2 = \frac{1}{2|\cos\theta|} \left(\frac{d}{d\theta} \{H^{*2} \cos\theta\} \right)^2. \quad (149)$$

In contrast to the corresponding small- k solution in the case $U = 0$ described in §5.1 this solution is uniformly valid.

7.2 The limit $k \rightarrow \infty$

In the limit $k \rightarrow \infty$ when $Q_R < Q < Q_C$ we have

$$\theta_{e1R} = \frac{3(U - H_0^* - H_0^{*2})}{H_0^*(H_0^{*3} + 3H_0^{*2} - 3UH_0^* - 6U)} \frac{1}{k} + O\left(\frac{1}{k^2}\right), \quad (150)$$

where $H_0^* = H^*(0)$, and the behaviour of H^* , H and h in the partially yielded zone $|\theta| \leq \theta_{e1R}$ is given by

$$H^* = H_0^* + O\left(\frac{1}{k^2}\right), \quad (151)$$

$$H = 1 + H_0^* - \left[1 - \left(\frac{\theta}{\theta_{e1R}} \right)^2 \right]^{\frac{1}{2}} + O\left(\frac{1}{k^2}\right), \quad (152)$$

$$h = 1 + H_0^* + O\left(\frac{1}{k^2}\right), \quad (153)$$

analogous to the corresponding large- k solution in the case $U = 0$ described in §5.2.

Similarly when $Q_R < Q \leq Q_C$ we also have

$$\theta_{e1L} = \pi - \frac{3(U + H_0^* + H_0^{*2})}{H_0^*(H_0^{*3} + 3H_0^{*2} + 3UH_0^* + 6U)} \frac{1}{k} + O\left(\frac{1}{k^2}\right), \quad (154)$$

where $H_0^* = H^*(\pi)$, and the behaviour of H^* , H and h in the partially yielded zone $|\pi - \theta| \leq \pi - \theta_{e1L}$ is given by

$$H^* = H_0^* + O\left(\frac{1}{k^2}\right), \quad (155)$$

$$H = 1 + H_0^* - \left[1 - \left(\frac{\pi - \theta}{\pi - \theta_{e1L}} \right)^2 \right]^{\frac{1}{2}} + O\left(\frac{1}{k^2}\right), \quad (156)$$

$$h = 1 + H_0^* + O\left(\frac{1}{k^2}\right), \quad (157)$$

again analogous to the corresponding large- k solution in the case $U = 0$ described in §5.2. Moreover,

$$\theta_{e2} = \theta_e^* - \frac{\cos^3 \theta_e^*}{2 \sin^2 \theta_e^*} \frac{1}{k} + O\left(\frac{1}{k^2}\right), \quad (158)$$

and the behaviour of H^* , H and h in the partially yielded zones $\theta_{e2R} \leq \theta \leq \theta_{eR}^*$ and $\theta_{eL}^* \leq \theta \leq \theta_{e2L}$, is given by

$$H^* = \frac{S \cos \theta_e^*}{2 \sin \theta_e^*} \frac{1}{k} + O\left(\frac{1}{k^2}\right), \quad (159)$$

$$H = \frac{S}{\cos \theta_e^*} \left[1 - \left(1 - \left\{ \frac{\theta_e^* - \theta}{\theta_e^* - \theta_{e2}} \right\}^2 \right)^{\frac{1}{2}} \right] + O\left(\frac{1}{k}\right), \quad (160)$$

$$h = \frac{S}{\cos \theta_e^*} + O\left(\frac{1}{k^2}\right). \quad (161)$$

Figure 29 shows a sketch of the leading-order solution in these partially yielded zones in which h and H^* are constant (independent of θ) whereas H has a semi-elliptical shape with width $O(k^{-1})$ and height $1/|\cos \theta_e^*|$. The solution for H (but not for H^* or h) is not uniformly valid when $\theta - \theta_e^* = O(1/k^2)$. This non-uniformity is resolved by an appropriate inner solution near $\theta = \theta_e^*$ satisfying $H'(\theta_e^*) = H'^*(\theta_e^*)$.

8 Conclusions

In this paper we considered the steady two-dimensional thin-film flow of a viscoplastic material, modelled as a biviscosity fluid with a yield stress, round the outside of a large horizontal stationary or rotating cylinder. In both cases we determined the leading-order solution both when $\lambda = O(1)$ as $\epsilon \rightarrow 0$ and in the distinguished limit $\lambda \rightarrow 0$

and $\epsilon \rightarrow 0$ in which $k = \epsilon/\lambda = O(1)$. When $\lambda = O(1)$ the flow consists, in general, of a region of yielded fluid (region 2) adjacent to the cylinder and a region of unyielded fluid (region 1) adjacent to the free surface, separated by $z = H$. In the distinguished limit the flow consists, in general, of a region of yielded fluid (region 2) adjacent to the cylinder whose stress is $O(1)$ above the yield stress and a pseudo-plug region adjacent to the free surface, in which the leading-order azimuthal component of velocity is independent of the radial coordinate but varies azimuthally, separated by $z = H^*$; the pseudo-plug region is itself, in general, divided by $z = H$ into a region of yielded fluid (region 3) whose stress is $O(\epsilon)$ above the yield stress and an unyielded region (region 1) adjacent to the free surface.

The solution for a stationary cylinder represents a curtain of fluid with prescribed volume flux Q falling onto the top of and off at the bottom of the cylinder. If $Q \leq \lambda/3$ then the flow is unyielded everywhere (type I), but when $Q > \lambda/3$ there is a yielded zone (type II). In the distinguished limit region 2 always extends all the way round the cylinder, but region 1 does so only when $Q \leq 1/2k$.

For a rotating cylinder a solution representing a film with finite thickness everywhere is possible only when the flux is sufficiently small. If $U \leq \lambda$ and $Q \leq Q_N$ or $U > \lambda$ and $Q \leq Q_R$ then the flow is unyielded everywhere (type I), if $U > \lambda$ and $Q_R < Q \leq \min(Q_C, Q_L)$ then there is a yielded zone on the right but not on the left (type II), while if $U > \lambda$ and $Q_L < Q \leq Q_C$ then there are yielded zones on both the right and left (type III). At the critical maximum flux ($Q = Q_N$ when $U \leq \lambda$ and $Q = Q_C$ when $U > \lambda$) the maximum supportable weight of fluid on the cylinder is attained and H^* , H and h all have a corner at $\theta = 0$. In the distinguished limit we have $Q_R = Q_L$ (so that flows of type II do not occur) and there are rigid plugs (absent

in the stationary case) near the top and bottom of the cylinder.

Acknowledgements

All three authors gratefully acknowledge invaluable discussions with Dr S. D. R. Wilson (Department of Mathematics, University of Manchester) during the course of the present work. In particular, the authors wish to thank Dr Wilson for providing them with a copy of his most recent paper (Wilson 1999) prior to its publication. The first author (A.B.R.) wishes to express his gratitude to the Carnegie Trust for the Universities of Scotland for their financial support via a Carnegie Scholarship. This work was begun while the second author (S.K.W.) was a Visiting Scholar in the Department of Engineering Sciences and Applied Mathematics of Northwestern University where he was partially supported under a United States Department of Energy Grant in the Basic Energy Sciences while he was visiting Prof. S. G. Bankoff and Prof. S. H. Davis.

References

- BALMFORTH, N. J. & CRASTER, R. V. 1999 A consistent thin-layer theory for Bingham plastics *J. Non-Newtonian Fluid Mech.* **84**, 65–81.
- BARNES, H. A. 1999 The yield stress — a review or ‘*παντα ρει*’ — everything flows? *J. Non-Newtonian Fluid Mech.* **81**, 133–178.
- BEVERLY, C. R. & TANNER, R. I. 1992 Numerical analysis of three-dimensional Bingham plastic flow. *J. Non-Newtonian Fluid Mech.* **42**, 85–115.
- BIRD, R. B., DAI, G. C. & YARUSSO, B. J. 1983 The rheology and flow of viscoplastic materials. *Rev. Chem. Eng.* **1**, 1–70.

- BURGESS, S. L. & WILSON, S. D. R. 1996 Spin-coating of a viscoplastic material. *Phys. Fluids* **8**, 2291–2297.
- COUSSOT, P. 1994 Steady, laminar, flow of concentrated mud suspensions in an open channel. *J. Hydr. Res.* **32**, 535–559.
- COUSSOT, P. & PROUST, S. 1996 Slow, unconfined spreading of a mudflow. *J. Geophys. Res.* **101**, 25217–25229.
- DI FEDERICO, V. 1998 Permanent waves in slow free-surface flow of a Herschel-Bulkley fluid. *Meccanica* **33**, 127–137.
- DUFFY, B. R. & WILSON, S. K. 1999 Thin-film and curtain flows on the outside of a rotating horizontal cylinder. *J. Fluid Mech.* **394**, 29–49.
- GANS, R. F. 1999 On the flow of a yield strength fluid through a contraction. *J. Non-Newtonian Fluid Mech.* **81**, 183–195
- HUANG, X. & GARCIA, M. H. 1997 A perturbation solution for Bingham-plastic mudflows. *J. Hydraul. Engng. ASCE* **123**, 986–994.
- HUANG, X. & GARCIA, M. H. 1998 A Herschel-Bulkley model for mud flow down a slope. *J. Fluid Mech.* **374**, 305–333.
- LIPSCOMB, G. G. & DENN, M. M. 1984 Flow of Bingham fluids in complex geometries. *J. Non-Newtonian Fluid Mech.* **14**, 337–346.
- LIU, K. F. & MEI, C. C. 1989 Slow spreading of a sheet of Bingham fluid on an inclined plane. *J. Fluid Mech.* **207**, 505–529.
- LIU, K. F. & MEI, C. C. 1990 Approximate equations for the slow spreading of a thin sheet of Bingham plastic fluid. *Phys. Fluids A* **2**, 30–36.
- LIU, K. F. & MEI, C. C. 1994 Roll waves on a layer of a muddy fluid flowing down a gentle slope - a Bingham model. *Phys. Fluids* **6**, 2577–2590.

- MOFFATT, H. K. 1977 Behaviour of a viscous film on the outer surface of a rotating cylinder. *J. Méc.* **16**, 651-673.
- NUSSELT, W. 1916a Die Oberflächenkondensation des Wasserdampfes. *Z. Vereines deutscher Ingenieure* **60**, 541-546.
- NUSSELT, W. 1916b Die Oberflächenkondensation des Wasserdampfes. *Z. Vereines deutscher Ingenieure* **60**, 569-575.
- O'DONOVAN, E. J. & TANNER, R. I. 1984 Numerical study of the Bingham squeeze film problem. *J. Non-Newtonian Fluid Mech.* **15**, 75-83.
- TICHY, J. A. 1991 Hydrodynamic lubrication theory for the Bingham plastic flow model. *J. Rheol.* **35**, 477-496.
- WALTON, I. C. & BITTLESTON, S. H. 1991 The axial flow of a Bingham plastic in a narrow eccentric annulus. *J. Fluid Mech.* **222**, 39-60.
- WILSON, S. D. R. 1993 Squeezing flow of a Bingham material. *J. Non-Newtonian Fluid Mech.* **47**, 211-219.
- WILSON, S. D. R. 1999 A note on thin-layer theory for Bingham plastics. *J. Non-Newtonian Fluid Mech.* **85**, 29-33.

Appendix - Derivation of the Governing Equations in the Distinguished Limit $k = \epsilon/\lambda = O(1)$

In this appendix we follow the approach outlined in the recent paper by Wilson (1999) to obtain the leading-order equations describing the present problems in the distinguished limit $\lambda \rightarrow 0$ and $\epsilon \rightarrow 0$ with $k = \epsilon/\lambda = O(1)$. As Wilson (1999) describes, in general the solution in this limit has three regions (in which the dependent variables are

hereafter denoted by the subscript 1, 2 or 3 as appropriate). In region 2 ($0 \leq z < H^*$) the fluid is yielded with $u_z = O(1)$, in region 3 ($H^* \leq z < H$) the fluid is yielded with $u_z = O(\epsilon)$ and in region 1 ($H \leq z \leq h$) the fluid is unyielded with $u_z = O(\epsilon)$, where $z = H^*(x)$, $z = H(x)$ and $z = h(x)$ are the unknown pseudo-yield surface, yield surface and free surface respectively.

In this Appendix we consider the general case of flow driven by body forces $G = G(x)$ and $F = F(x)$ in the x and z directions respectively. Non-dimensionalising appropriately in the unyielded region the governing equations are

$$u_x + w_z = 0, \quad (162)$$

$$\epsilon p_x = \lambda^{-1}(\epsilon^2 u_{xx} + u_{zz}) + G, \quad (163)$$

$$p_z = \epsilon \lambda^{-1}(\epsilon^2 w_{xx} + w_{zz}) + F, \quad (164)$$

and the normal and tangential stresses on any surface $z = f(x)$ are given by

$$-p + \frac{2\epsilon\lambda^{-1}}{1 + \epsilon^2 f_x^2} [\epsilon^2 f_x^2 u_x + w_z - f_x(\epsilon^2 w_x + u_z)], \quad (165)$$

$$\frac{\lambda^{-1}}{1 + \epsilon^2 f_x^2} [(1 - \epsilon^2 f_x^2)(\epsilon^2 w_x + u_z) + 2\epsilon^2 f_x(w_z - u_x)], \quad (166)$$

respectively, while in the yielded regions the governing equations are

$$u_x + w_z = 0, \quad (167)$$

$$\epsilon p_x = \left[1 + \frac{1 - \lambda}{q}\right] (\epsilon^2 u_{xx} + u_{zz}) - \frac{(1 - \lambda)}{q^2} [2\epsilon^2 u_x q_x + (u_z + \epsilon^2 w_x) q_z] + G, \quad (168)$$

$$p_z = \left[1 + \frac{1 - \lambda}{q}\right] \epsilon (\epsilon^2 w_{xx} + w_{zz}) - \frac{(1 - \lambda)}{q^2} \epsilon [(\epsilon^2 w_x + u_z) q_x + 2w_z q_z] + F, \quad (169)$$

and the normal and tangential stresses on any surface $z = f(x)$ are given by equations (165) and (166) with λ^{-1} replaced by $1 + (1 - \lambda)/q$, respectively. The local shear rate q is given by

$$q = [4\epsilon^2 u_x^2 + (u_z + \epsilon^2 w_x)^2]^{\frac{1}{2}} \quad (170)$$

and the yield condition is

$$q = \lambda \quad (171)$$

on the yield surface $z = H$.

In region 1 (unyielded fluid with $u_z = O(\epsilon)$)

$$u_1 = u_{10}(x) + \epsilon u_{11}(x, z) + O(\epsilon^2), \quad (172)$$

$$q_1 = q_{10} + \epsilon q_{11} + O(\epsilon^2), \quad (173)$$

where from (170) we obtain $q_{10} = 0$ and

$$q_{11} = [4u_{10,x}^2 + u_{11,z}^2]^{\frac{1}{2}}. \quad (174)$$

From (162)–(164) we obtain the leading-order governing equations

$$u_{10,x} + w_{10,z} = 0, \quad (175)$$

$$ku_{11,zz} + G = 0, \quad (176)$$

$$p_{10,z} - F = 0. \quad (177)$$

In region 2 (yielded fluid with $u_z = O(1)$)

$$u_2 = u_{20}(x, z) + \epsilon u_{21}(x, z) + O(\epsilon^2), \quad (178)$$

$$q_2 = q_{20} + \epsilon q_{21} + O(\epsilon^2), \quad (179)$$

where from (170) we obtain $q_{20} = -Su_{20,z}$ and $q_{21} = -Su_{21,z}$ where $S = -\text{sgn}(u_{20,z})$.

From (167)–(169) we obtain the leading-order governing equations

$$u_{20,x} + w_{20,z} = 0, \quad (180)$$

$$u_{20,zz} + G = 0, \quad (181)$$

$$p_{20,z} - F = 0. \quad (182)$$

In region 3 (yielded fluid with $u_z = O(\epsilon)$)

$$u_3 = u_{30}(x) + \epsilon u_{31}(x, z) + O(\epsilon^2), \quad (183)$$

$$q_3 = q_{30} + \epsilon q_{31} + O(\epsilon^2), \quad (184)$$

where from (170) we obtain $q_{30} = 0$ and

$$q_{31} = [4u_{30,x}^2 + u_{31,z}^2]^{\frac{1}{2}}. \quad (185)$$

From (167)–(169) we obtain the leading-order governing equations

$$u_{30,x} + w_{30,z} = 0, \quad (186)$$

$$\left(\frac{u_{31,z}}{q_{31}} \right)_z + G = 0, \quad (187)$$

$$p_{30,z} + 2 \frac{w_{30,z} q_{31,z}}{q_{31}^2} - F = 0. \quad (188)$$

At the solid substrate $z = 0$ there is no slip and so at leading order

$$u_{20} = U, \quad (189)$$

$$w_{20} = 0. \quad (190)$$

The pseudo-yield surface $z = H^*(x)$ is the surface at which

$$u_{20,z} = 0 \quad (191)$$

(or, equivalently, $u_{31,z} \rightarrow \infty$) and separates region 3 (yielded fluid with $u_z = O(\epsilon)$) from region 2 (yielded fluid with $u_z = O(1)$). At the pseudo-yield surface the velocity, normal and tangential stress components are continuous and so at leading order

$$u_{20} = u_{30}, \quad (192)$$

$$w_{20} = w_{30}, \quad (193)$$

$$-p_{20} = -p_{30} + 2 \frac{w_{30,z}}{q_{31}}, \quad (194)$$

$$-S = \frac{u_{31,z}}{q_{31}}. \quad (195)$$

The yield surface $z = H(x)$ separates region 1 (unyielded fluid with $u_z = O(\epsilon)$) from region 3 (yielded fluid with $u_z = O(\epsilon)$). At leading order the yield condition (171) gives $q_{31} = 1/k$, that is

$$4u_{30,x}^2 + u_{31,z}^2 = \frac{1}{k^2}. \quad (196)$$

At the yield surface the velocity, normal and tangential stress components are continuous and so at leading order

$$u_{10} = u_{30}, \quad (197)$$

$$w_{10} = w_{30}, \quad (198)$$

$$-p_{10} = -p_{30}, \quad (199)$$

$$u_{11,z} = u_{31,z}. \quad (200)$$

At the free surface $z = h(x)$ the normal and tangential stress components are continuous and so at leading order

$$-p_{10} + 2kw_{10,z} = 0, \quad (201)$$

$$ku_{11,z} = 0. \quad (202)$$

Solving (181) for u_{20} subject to (189) at $z = 0$ and (191) at $z = H^*$ yields

$$u_{20} = U + \frac{G}{2}(2H^* - z)z. \quad (203)$$

Thus from (192) and (197)

$$u_{10} = u_{30} = U + \frac{G}{2}H^{*2} \quad (204)$$

and so at leading order the volume flux is given by

$$Q = \int_0^{H^*} u_{20} dz + (H - H^*)u_{30} + (h - H)u_{10} = Uh + \frac{G}{6}(3h - H^*)H^{*2}. \quad (205)$$

If required, the corresponding solutions for w_{10} , w_{20} and w_{30} can then be calculated by solving equations (175), (180) and (186) subject to (190) at $z = 0$, (193) at $z = H^*$ and (198) at $z = H$. Solving (177) for p_{10} subject to (201) at $z = h$ yields

$$p_{10} = -(h - z)F - 2ku_{10,x}, \quad (206)$$

so solving (188) for p_{30} subject to (199) at $z = H$ yields

$$p_{30} = -(h - z)F - 2\frac{u_{30,x}}{q_{31}}, \quad (207)$$

and then solving (182) for p_{20} subject to (194) at $z = H^*$ yields

$$p_{20} = -(h - z)F. \quad (208)$$

Solving (176) for $u_{11,z}$ subject to (202) at $z = h$ yields

$$u_{11,z} = \frac{1}{k}(h - z)G, \quad (209)$$

so solving (187) for $u_{31,z}$ subject to (200) at $z = H$ yields

$$u_{31,z} = q_{31}(h - z)G. \quad (210)$$

Using these solutions the tangential stress condition (195) at $z = H^*$ yields

$$(h - H^*)|G| = 1, \quad (211)$$

and the yield condition (196) at $z = H$ gives

$$(h - H)^2 G^2 + k^2 \left[\frac{d}{dx} \{H^{*2}G\} \right]^2 = 1. \quad (212)$$

The stress is given by

$$\tau = kq_{11} + O(\epsilon) \quad (213)$$

in region 1, by

$$\tau = 1 + q_{20} + O(\epsilon) \quad (214)$$

in region 2 and by

$$\tau = 1 + \left[q_{31} - \frac{1}{k} \right] \epsilon + O(\epsilon^2) \quad (215)$$

in region 3. In particular, (215) shows that the stress is only $O(\epsilon)$ above the yield value of unity throughout region 3.

Equations (205), (211) and (212) (the volume-flux, pseudo-yield and yield conditions respectively) are three equations for the three unknown surfaces H^* , H and h . The case of gravity-driven flow round a stationary cylinder discussed in §5 is recovered by identifying x with α and taking $G = \sin \alpha$, $F = -\cos \alpha$ and $S = -1$, while the corresponding case for flow round a rotating cylinder discussed in §7 is recovered by identifying x with θ and taking $G = -\cos \theta$, $F = -\sin \theta$ and $S = \text{sgn}(\cos \theta)$. The case of pressure-driven flow in a channel considered by Wilson (1999) corresponds to setting $F = 0$, $G = 0$ and rescaling the pressure p (with, of course, different boundary conditions); a rather more direct but ad hoc procedure is simply to set $F = 0$ and $G = -dp/dx$ in the leading-order equations.

Figure Captions

FIGURE 1. The biviscosity model.

FIGURE 2. Locally rectilinear flow on a locally planar substrate inclined at an angle $\alpha = \pi/2 - \theta$ to the horizontal moving parallel to itself with speed U when (a) $\lambda = O(1)$, and (b) in the distinguished limit $\lambda \rightarrow 0$ and $\epsilon \rightarrow 0$ with $k = \epsilon/\lambda = O(1)$.

FIGURE 3. Leading-order solutions for flow round a large stationary cylinder (including typical streamlines) illustrating (a) a flow of type I when $Q = 2/25$ and $\lambda = 1/4$, and (b) a flow of type II when $Q = 1$ and $\lambda = 1/4$.

FIGURE 4. Plots of H (lower curves) and h (upper curves) as functions of α/π when $Q = 1$ for $\lambda = 0, 1/100, 1/10, 1/2$ and 1 . Note that the solutions for h in the cases $\lambda = 0$ and $\lambda = 1/100$ are virtually indistinguishable at this scale.

FIGURE 5. Plots of H (lower curves) and h (upper curves) as functions of α/π when $\lambda = 1/4$ for $Q = 1/40, 1/12, 1/4, 1$ and 2 . Note that H is present only when $Q > \lambda/3 = 1/12$.

FIGURE 6. Plot of $\Delta h''(\alpha_e)$ as a function of λ for $Q = 1/12, 1/6, 1/3, 1, 5$ and 10 .

FIGURE 7. Plots of the curves $Q = \lambda/3$ and $Q = Q_M$ (given parametrically by (52)) as functions of λ showing how they divide the (λ, Q) parameter plane into regions in which the flow is of type I, the flow is of type II with a maximum in H at $\alpha = \pi/2$ (labelled II_{\max}), and the flow is of type II with a minimum in H at $\alpha = \pi/2$ (labelled II_{\min}).

FIGURE 8. Plot of the weight on the right-hand side of the cylinder W as a function of Q for a range of values of λ .

FIGURE 9. Leading-order solutions for flow round a large stationary cylinder in the distinguished limit described in §5 illustrating (a) a flow of type II_1 when $Q = 1$ and $k = 9/20$, and (b) a flow of type II_2 when $Q = 1$ and $k = 2$.

FIGURE 10. Plots of H^* , H and h as functions of α/π when $Q = 1/10$ for $k = 1, 5/2, 5, 15/2, 10, 20, 50$ and 100 . Note that H^* and h are independent of k .

FIGURE 11. Plots of H^* , H and h as functions of α/π when $Q = 1$ for $k = 1/10, 1/4, 1/2, 3/4, 1, 5/2, 10$ and 50 . Note that H^* and h are independent of k .

FIGURE 12. Plots of H^* , H and h as functions of α/π when $Q = 10$ for $k = 1/100, 1/40, 1/20, 1/10, 1/4, 1/2, 1$ and 10 . Note that H^* and h are independent of k .

FIGURE 13. Sketch of the leading-order solutions for H^* , H and h near $\alpha = \pi/2$ in the limit $k \rightarrow \infty$.

FIGURE 14. Sketch of the first-order-accurate solutions for H^* , H and h near $\alpha = \pi/2$ in the limit $Q \rightarrow \infty$.

FIGURE 15. Leading-order solutions for flow round a large rotating cylinder (including streamlines) illustrating (a) a flow of type I when $Q = 9/10$, $\lambda = 1/2$ and $U = 1$, (b) a flow of type II when $Q = 7/4$, $\lambda = 1/2$ and $U = 8/5$, and (c) a flow of type III when $Q = 21/5$, $\lambda = 1/2$ and $U = 3$.

FIGURE 16. Plot of the (U, Q) parameter plane for the case $\lambda = 1/2$ showing how the curves $Q = Q_N$, $Q = Q_R$, $Q = Q_L$ and $Q = Q_C$ divide the parameter plane into regions in which either there is no solution or the flow is of type I, II or III.

FIGURE 17. Plots of H (lower curves) and h (upper curves) as functions of θ/π when $U = 19/10$ and $Q = 2$ for $\lambda = 0, 1/10, 3/10$ ($Q = Q_L$), $1/2$ and 0.714225 ($Q = Q_C$).

FIGURE 18. Plots of H (lower curves) and h (upper curves) as functions of θ/π when $\lambda = 1/2$ and $Q = 3$ for $U = 2.34296$ ($Q = Q_C$), $5/2$, $17/6$ ($Q = Q_L$), 3 , $19/6$ ($Q = Q_R$) and $7/2$.

FIGURE 19. Plots of H (lower curves) and h (upper curves) as functions of θ/π when $\lambda = 1/2$ and $U = 3$ for $Q = 5/2$, $17/6$ ($= Q_R$), 3 , $19/6$ ($= Q_L$), $7/2$, 4 and $17/4$ ($= Q_C$).

FIGURE 20. Plots of A and $h'(\theta_{eR})$ as functions of U for a range of values of λ . The curve $[U/3(1+U)]^{1/2}$ and the constant value $6^{-1/2}$ are shown with dashed lines.

FIGURE 21. Plot of the (U, Q) parameter plane for the case $\lambda = 1/2$ showing how the curve $Q = Q_M$ divides the region of the parameter plane in which the flow is of type III into regions in which the flow is of type III with a maximum in H at $\theta = \pi$ (labelled III_{max}) and the flow is of type III with a minimum in H at $\theta = \pi$ (labelled III_{min}). Note that on this scale the curves $Q = Q_R$ and $Q = Q_L$ are indistinguishable from one another and the curve $Q = Q_N$ is not visible.

FIGURE 22. Plot of the weight on the cylinder W as a function of Q for a range of values of U in the case $\lambda = 1/2$.

FIGURE 23. Plot of the maximum supportable weight on the cylinder W_{\max} as a function of U for a range of values of λ . The constant value 4.44272 is shown with a dashed line.

FIGURE 24. Plot of the (U, Q) parameter plane for the case $\lambda = 0$ showing how the curves $Q = Q_R = Q_L$ and $Q = Q_C$ divide the parameter plane into regions in which either there is no solution or the flow is of type I or III.

FIGURE 25. Leading-order solutions for flow round a large rotating cylinder in the distinguished limit described in §7 illustrating (a) a flow of type III₁ when $U = 2$, $Q = 3$ and $k = 5/4$, (b) a flow of type III₂ when $U = 2$, $Q = 3$ and $k = 3/2$, and (c) a flow of type III₃ when $U = 2$, $Q = 3$ and $k = 3$.

FIGURE 26. Plots of H^* , H and h as functions of θ/π when $U = 2$ and $Q = 3$ for $k = 2/5, 7/10, 1, 5/4, 13/10, 27/20, 3/2, 2, 5/2, 11/4, 3$ and $7/2$. Note that H^* and h are independent of k .

FIGURE 27. Plots of H^* , H and h as functions of θ/π when $U = 2$ and $Q = 19/6$ ($= Q_C$) for $k = 3/10, 2/5, 1/2, 0.566947$ ($= k_{\text{critR}}$), $13/20, 5/4, 7/4, 2, 9/4, 5/2$ and 3 . Note that H^* and h are independent of k .

FIGURE 28. Plot of B as a function of k for a range of values of U . The corresponding asymptotes $k = k_{\text{crit}}$ are denoted with dashed lines.

FIGURE 29. Sketch of the leading-order solutions for H^* , H and h near $\theta = \theta_e^*$ in the limit $k \rightarrow \infty$.

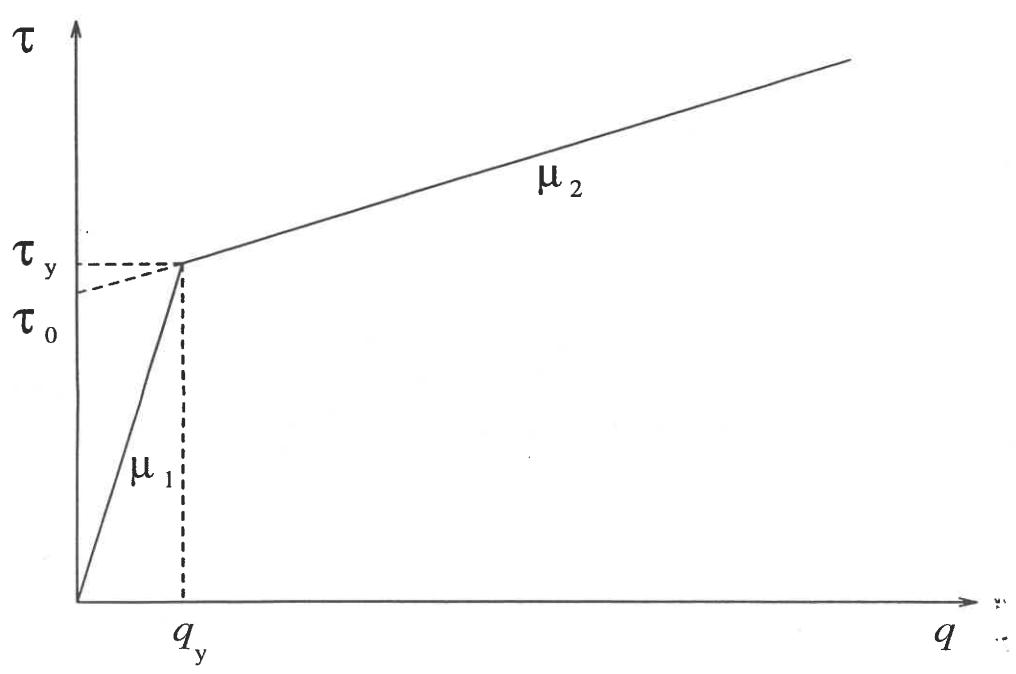


FIG 2(a)

